AN ABSTRACT OF THE THESIS OF

Steven Arthur Narkiewicz for the degree MASTER OF SCIENCE
(Name) (Degree)

in CIVIL ENGINEERING presented on Feb. 6, 1975
(Major Department) (Date)

Title: FLOW SLIDE CONTROL WITH SLOPE REVETMENTS

Abstract approved: Redacted for privacy
W. L. Schroeder

This paper examines the response of submerged model sand slopes to vibration and the beneficial effects of placing rock revetments on the face of the slope to prevent flow slides.

Pore water pressure response and deflection were used as a criteria for stability in an attempt to relate stability with dimensionless parameters describing the slope. It was possible to fit a linear relationship to the data so that the pore pressure response increased linearly with the dimensionless revetment thickness. It was also found that pore pressure response increased for decreasing steepness of the slope face for constant dimensionless revetment thickness.

Three distinct modes of failure were observed during the study. An empirical slope stability analogy was developed based on these failure modes which suggested a design procedure for determining the thickness of rock revetments required to prevent liquefaction flow slides. The design procedure was apparently very conservative for

the model slopes but the failure modes upon which the procedure was based remain to be verified in full size slopes.

Flow Slide Control with Slope Revetments

by

Steven Arthur Narkiewicz

A THESIS

submitted to

Oregon State University

in partial fulfillment of
the requirements for the
degree of

Master of Science

Completed February 6, 1975

Commencement June 1975

APPROVED:

Redacted for privacy

Associate Professor of Civil Engineering
in charge of major

Redacted for privacy

Head of Department of Civil Engineering

Redacted for privacy

Dean of Graduate School

Date thesis is presented Feb. 6, 1975

Typed by Mary Jo Stratton for Steven Arthur Narkiewicz

TABLE OF CONTENTS

LIST OF TABLES

LIST OF FIGURES

FLOW SLIDE CONTROL WITH SLOPE REVETMENTS

I. INTRODUCTION

The liquefaction of saturated sand is a condition whereby increased pore water pressures are induced by vibration caused volume change. If the pore pressure increase is large enough the effective stress in the sand is reduced to zero and the sand deposit becomes a fluid.

The study of sand liquefaction and its relationship to the damaging effects of flow slides on sand slopes caused by earthquakes has received little serious study. The problem is acute in deposits of loose, fine, saturated sands. Many private and public works are built and will continue to be built along waterways and in coastal areas where there are natural loose sand deposits. Cities such as Portland, Oregon, have historically reclaimed previously flooded land by constructing hydraulic fills utilizing uniform fine sands dredged from adjacent river channels. Besides the conventional problem of designing foundations on such loose deposits, there exists an unconventional problem of what to do about the possibility of earthquake induced flows in the slopes along the shoreline. Solutions to the problem of preventing liquefaction and the resulting flow slides on slopes have fallen into five general categories:

1) Densify the sand

2) Excavate and replace the sand

3) Cement the deposit with a chemical grout

4) Surcharge the material so that it cannot liquefy

5) Contain the mass which might liquefy so that no slide can occur

The first three alternatives tend to be expensive and are usually limited to applications where only small areas need to be treated. Surcharging and confinement with free draining rock revetments have been shown to decrease the harmful effects of liquefaction and could become economically viable choices in areas of moderate seismic risk, or where some building damage can be tolerated. The problem presented by this method, of course, if to find a rational procedure for designing the revetment. Previous laboratory studies have provided much information on liquefaction of sand under various stress conditions, but the results have not provided a useful means for defining the behavior of actual sand slopes. Scaled physical models may better serve the purpose of studying slope behavior. The possibility exists for simulating actual conditions in a slope more realistically than with the conventional approach of laboratory tests and analytical modeling using engineering mechanics. In this approach, the assumptions regarding physical model validity must be justified instead of the simplifying assumptions which usually accompany the alternative method.

II. PURPOSE AND SCOPE

The purpose of this study was to determine the effects of a free draining rock revetment on the liquefaction potential and flow slide generation in a saturated sand slope subject to internal shaking. Scale models of slopes were used in an attempt to define pore water pressure response and, hence, liquefaction potential, of real slopes in a more quantitative manner than previous laboratory studies. Similitude theory was used to develop basic dimensionless parameters governing liquefaction and flow of a model slope. Three different heights of slopes with varying thicknesses of gravel on the face and varying slope angles were subjected to internal vibration to determine if some regular relationship could be derived for the dimensionless variables. The primary objective of the study was to determine if the liquefaction and flow slide phenomenon could be scaled. If a valid scaling relationship could be developed it would then be possible to predict the thickness of a rock revetment needed to achieve various degrees of stabilization of real slopes.

III. THE LIQUEFACTION PHENOMENON

Documented Failures

Many flow slides induced by liquefaction have taken place in recent earthquakes, and they have been documented extensively. During the 1964 Alaska earthquake some of the most dramatic slides recorded destroyed the harbor facilities at both Valdez and Seward. Descriptions of these slides have been compiled by Seed (7), among others. In the town of Valdez as much as 700 feet of land immediately behind the original shoreline disappeared along 3200 feet of the harbor front. The Valdez dock and accompanying warehouses were on the land and slid into the bay. Lateral ground movements, cracks, fissures, and sand boils were seen extending as much as 3600 feet behind the slide line, indicating the vast area that had liquefied. Figures 1 and 2 show the extent of the slide in both plan and profile.

In Seward similar flow slides devastated boat harbors and docks and completely reshaped the shoreline. About 4000 feet of shoreline was affected and it is estimated that "the maximum depth of soil displaced by sliding was 120 feet" (7).

The slides in both Seward and Valdez were similar because initial conditions were much the same. According to Seed, both towns were located on deltiac deposits consisting of gravel, fine sand, and

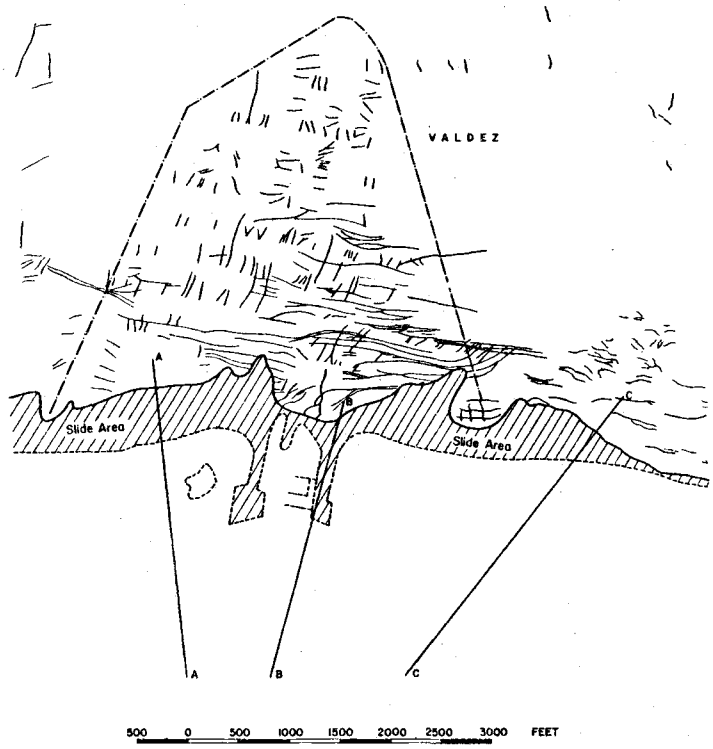

Figure 1. Map showing slide area and ground cracking at Valdez, Alaska.

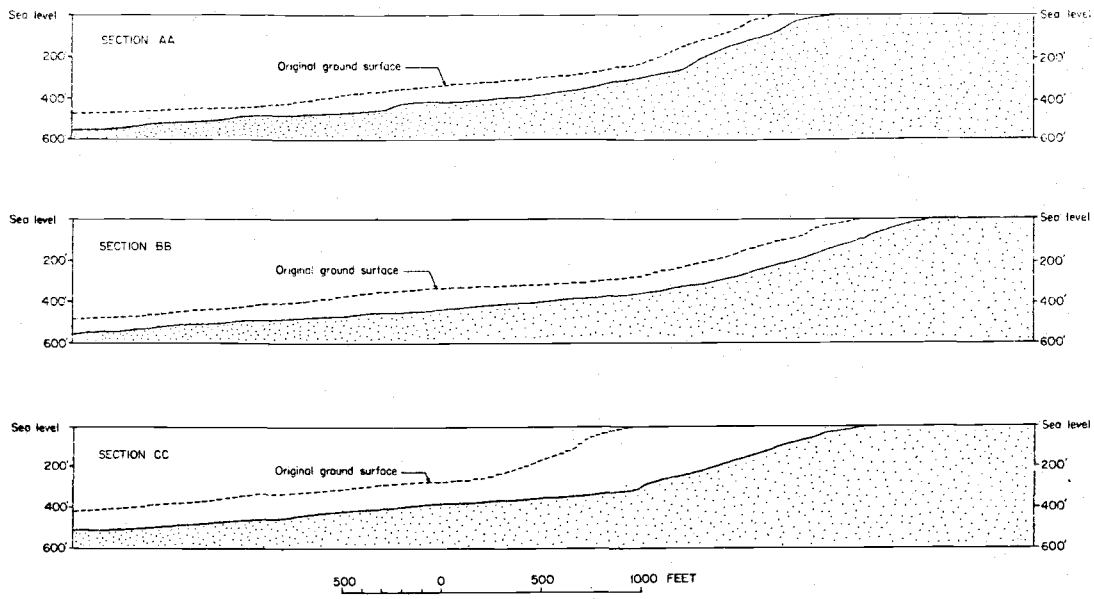

Figure 2. Profiles through slide area at Valdez, Alaska.

silt. In addition, Standard Penetration resistances were less than 20 blows per foot where they could be determined. The soils were submerged and therefore saturated.

Slides of the type that occurred in Seward and Valdez have occurred around the world where similar geologic conditions exist. The damage and loss of life caused by such slides heightened the interest in laboratory studies on the factors effecting liquefaction of sand.

Previous Laboratory Tests

Since the early 1960's extensive laboratory tests have been conducted to determine the behavior of sand under repetitive loading. Most of these tests have been conducted in altered triaxial shear devices. The methods of applying the simulated earthquake stresses have varied with different researchers but most of the procedures and results have been very similar. Seed and Lee (3, 4) conducted two series of cyclic loaded triaxial tests representing assumed stress conditions that would exist for a soil element subject to earthquake stress under a flat ground surface and under a slope. They investigated the various factors affecting the production of excess pore water pressures which can cause liquefaction. Sand samples were tested in undrained shear under varying conditions of relative density, initial confining pressure, initial effective principal stress ratio, and

magnitude of cyclic deviator stress. The tests were performed undrained, assuming that drainage would be unimportant initially in fine sands subject to a relatively short period of earthquake disturbance. Seed and Lee found generally that:

1) For conditions of an isotropically consolidated sample and constant magnitude of cyclic stress, higher excess pore pressures were produced for lower confining pressures or relative density;
2) For isotropically consolidated samples, increasing magnitudes of cyclic stress were necessary to liquefy sand samples with increasing relative density or increasing confining pressure; and
3) For anisotropically consolidated samples, increasing magnitudes of cyclic stress were necessary to liquefy sand samples with increasing ratios of effective principal stress.

Schroeder and Shuster (6) and Wen Xi (11) have also arrived at these conclusions but have found, in addition, that for the same magnitude of cyclic stress and relative density, higher excess pore pressures are produced for decreasing values of initial effective principal stress ratios. Schroeder and Shuster have also shown that the results of Seed and Lee regarding the effects of density and confining pressure for isotropic initial effective stress conditions also apply for initial effective principal stress ratios greater than 1. Therefore, for a

sample with a principal stress ratio of 2.0, for example, pore water pressure produced by cyclic loading will increase with decreasing density or decreasing confining pressure.

Mechanisms of Liquefaction

Using general results from the laboratory studies it should be possible to theorize a mechanism of liquefaction and flow for a submerged sand slope.

If a submerged sand slope consisting of loose, fine sand is subjected to earthquake shaking, the contacts between sand particles are momentarily disrupted. The sand, therefore, tends to densify. This tendency for volume decrease without drainage increases the pore water pressure. Since confining pressure is a minimum at the surface of the deposit and increases with depth, the sand should liquefy at the surface of the deposit initially. However, once the surface has liquefied, the effective stress on the layer below is reduced which also allows it to liquefy. This process could then supposedly proceed downward into the deposit until the intensity of shaking is damped enough so that liquefaction cannot occur. This mechanism has been described as progressive failure by Seed (7) and has been documented during the slide at Seward previously discussed. Witnesses saw strips of the shoreline progressively peel off and disappear into the bay.

Florin and Ivanov (2) have produced similar progressive failures in laboratory model tests. They vibrated a saturated sand sample imparting base motions with a shaking table. Their results are shown in Figure 3. The diagonal line in the figures represents complete liquefaction. From the figures it can be seen that liquefaction proceeded downward with time until the deposit was completely fluid, and then drainage caused pore pressure to drop and the layer solidified from the bottom up.

In a flat deposit progressive failure seems to only proceed to a limited depth (about 20 to 30 meters), reportedly because the ground accelerations decrease with depth (4). But a slope behaves differently. As the surface of a slope liquefies it is free to flow downhill, exposing an underlying layer to decreased confining pressure. Successive slices are then permitted to flow until the ground motion stops, the slope is reduced, or drainage allows pore water pressure to dissipate until effective stresses are high enough to stabilize the slope.

The liquefaction potential of the sand in a slope should also be affected by the original slope angle. Since laboratory tests have shown that pore water pressure generation is smaller for higher values of initial effective principal stress ratio, steeper slopes should be harder to liquefy than shallow slopes. This qualitative interpretation of repeated load test data has been confirmed by model test results reported in this study.

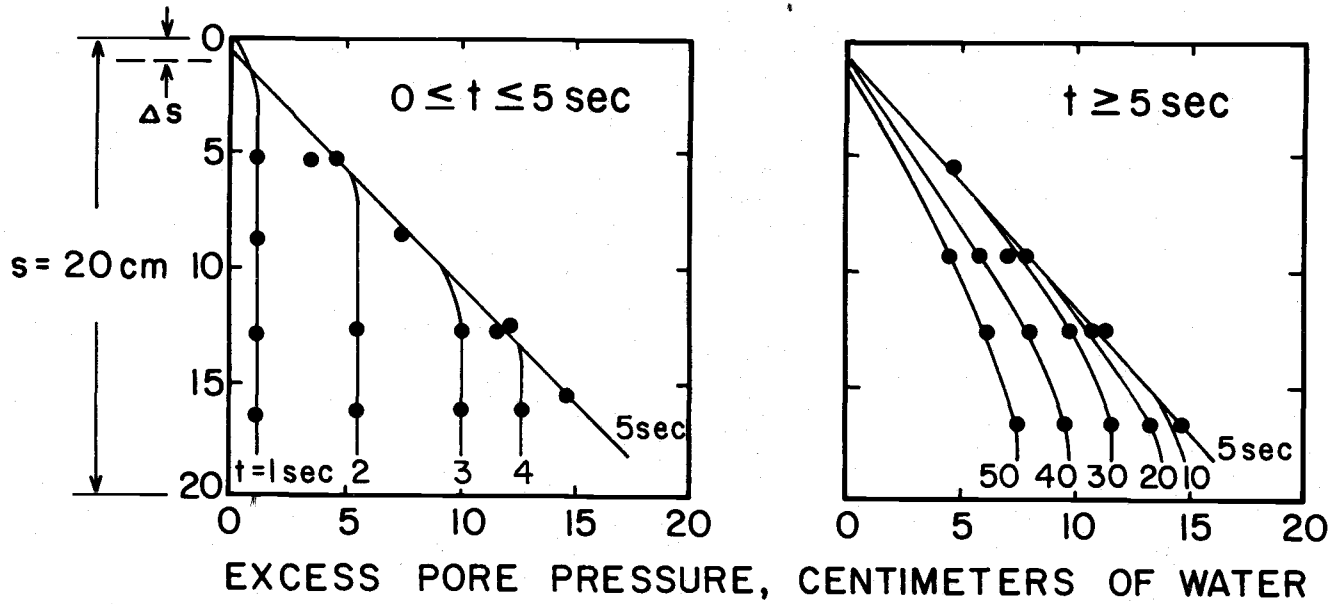

Figure 3. Distribution of excess pressure in a sand stratum acted on by vibrations.

High densities inhibit high pore water pressure generation. Therefore, if density should decrease with depth in a slope, it might be possible to liquefy a loose layer within the deposit before a confined dense surface layer would liquefy. The rise in pore pressure in the deep layer would initiate flow toward the surface causing liquefaction to proceed upward. Liquefaction, in this case, would be evidenced at the surface in the form of a sand boil.

Corrective Measures

The factors which affect liquefaction in a slope suggest measures that might be used to prevent the various failure mechanisms. To completely prevent a slope from liquefying it should be sufficiently surcharged with a free draining material to prevent surface liquefaction and flow, it should be sufficiently dense to prevent liquefaction at depth, and it should be sufficiently steep to minimize pore water pressure buildup. However, practical problems arise. The recurrence interval of the design earthquake in many instances may be too long to justify the expense of protective treatment of a large slope. In such cases it might be premissible to allow the deposit to liquefy during the design earthquake if only minor damage would result. If, for instance, a warehouse is to be constructed on a sand fill adjacent to a river, the need to prevent the entire deposit from liquefying may not exist. The settlement of the footings of a warehouse could

conceivably not be large enough to justify the expense. However, preventing the slope from flowing would be of paramount importance. Without some slope protection the warehouse might slide into the river and be destroyed, along with its contents. To accomplish this degree of stabilization might only require controlling the slope angle and placing a free draining blanket or revetment on the face of the slope. The revetment, according to interpretation of cyclic shear tests, should accomplish one of two desirable objectives. It should prevent liquefaction on the slope face and, therefore, prevent flows which initiate at the surface. Additionally, because of its strength it would act like a buttress to contain the liquefied mass that could develop behind the slope crest. The model slopes described in this study were failed in order to test these hypotheses.

The Alternatives

Generally, there are three possible approaches to studying the problem of liquefaction and liquefaction induced sliding in saturated sand slopes. The first and most desirable method is to study the failure of real sand slopes *in situ*. The second is to study liquefaction tendencies of slope materials in the laboratory and then use the data for input to deterministic models of slope failure using engineering mechanics. The third is to study scale model slopes and attempt to relate their behavior to real slopes.

Naturally, the most correct method of studying the effect of a revetment on the liquefaction to slopes would be to instrument and revet real slopes and then to wait for an earthquake to supply the excitation necessary to cause the slope to respond. The advantages of such a scheme are obvious. The soil is completely free to react to real stresses under real conditions of drainage, confining pressure, density and stratigraphy. The measured response of such slopes could be used directly in a design criteria for reveting slopes against failure. There would be no need to account for assumptions and approximations needed in theories developed using laboratory tests. However, the disadvantages of instrumenting case studies explains why the method is not used more often. While it is desirable to study slopes under in situ conditions, it would be necessary to conduct a large number of tests to encompass all of the variations in soil properties and other conditions that could represent different deformation and liquefaction characteristics. Of course, it also might take several hundred years to collect all of these data since the occurrence of earthquakes is irregular and unpredictable. It is obvious, then, that this type of study, while not impossible, it just not practical.

Another approach would be to employ quantitative data on soil behavior from laboratory studies already performed to develop a slope stability analysis model using engineering mechanics. The advantages of this approach include the relative simplicity and economy

of testing small samples in a laboratory and again, the ability to possibly develop a revetment design criteria by extending the laboratory data to real slope conditions.

The basic disadvantages of this approach include the problems of accounting for simplifying assumptions and questions related to the ability of the laboratory test to simulate actual field conditions. Although the qualitative and the quantitative response of sand to repetitive loading in the laboratory has been used to predict liquefaction potential of flat saturated sand deposits in the field, the simulation of stresses and drainage for slopes in the laboratory is a comparatively more difficult problem (7). Various researchers feel that the best simulation of field conditions so far has been achieved using special triaxial shear and simple shear tests, but they also admit that their results probably underpredict the stresses that produce liquefaction in the field (1, 5, 9). There is a further stumbling block in that results of laboratory tests on samples representing small parts of a large slope cannot easily be translated to a rational mechanistic behavior of slopes when no general failure criterion has been developed. Triaxial test results simply cannot duplicate the development of a liquefaction slide in a slope.

In more general terms, it is extremely difficult thus far to accept with any certainty that undrained repetitive load shear tests on small samples represent the complex situations of stress and drainage

which take place within a sand slope in the field. Furthermore, while it is uncertain whether actual field stresses are simulated in laboratory tests, it is certain that the assumption of undrained shear does not simulate real conditions and would probably lead to overly conservative designs of the rock revetment needed to stabilize liquefied slopes. The application of laboratory test results to actual slope conditions, then, is a very complex problem and the state of the art has not progressed sufficiently at this time to extrapolate lab results to field behavior in a quantitative manner.

The complex nature of the stabilization of slopes against flow lends itself to another method of studying the problem--model studies. The purpose of a model study is to find a functional relationship for a complex phenomenon by testing scale models in the laboratory and plotting the results in terms of the dimensionless parameters which describe the phenomenon. This method is particularly useful when the functional relationship is too complex to be analyzed using physical laws and mechanics. In the case of modeling the effect of a revetment on the liquefaction potential of a slope, it may be possible to better represent actual conditions of drainage and stress and also to establish a failure mode for other analyses.

There are, however, serious objections to modeling dynamic soil behavior in saturated sands (10). The strength properties of sand are pressure dependent and, therefore, it is argued that the

behavior of small slopes will be significantly different from large slopes. Permeability characteristics are also difficult to model. The acceleration produced by earthquake ground shaking is difficult to simulate in a model, and therefore simplifying assumptions must be made as to the proper excitation to use to best represent an earthquake.

All of these objections are valid but the magnitude of their effects on model studies is subject to speculation. In comparing model slopes with heights of 40, 80, and 100 cm, it may be possible to ignore some of these objections because the differences in model sizes are not drastic. Of course, extrapolating the results of tests on these models to full sized slopes requires caution and the necessity to perhaps test full scale slopes in some manner to see if small scale relationships can be used. In any case, this study was carried out to see if scale models might offer another useful alternative to case studies and laboratory tests for studying flow slides and the effects of revetments. The success of the study depends on the ability to find a functional relationship between the stability of the revetted slope and the dimensionless parameters derived to describe the slope.

IV. SLOPE TESTING

Modeling of Slopes

The dimensionless parameters describing the stability of a sand slope covered with a rock revetment can be developed using dimensional analysis. Figure 4 shows such a slope and the physical parameters which describe constituent materials.[1] Assuming that the stability of the slope is

$$f(\phi,\ \gamma,\ \gamma_w,\ k,\ A_x,\ Ay,\ \eta\ t,\ H,\ B,\ \phi_1,\ k_1,\ \gamma_1,\ z)$$

dimensional analysis yields

$$\text{Stability} = f(\phi,\ \phi_1,\ \frac{\gamma}{\gamma_w},\ \frac{H}{A_x},\ \frac{H}{A_y},\ \frac{k}{H\eta},\ \frac{H}{kt},\ \frac{H}{B},\ \frac{\gamma}{\gamma_1},\ \frac{k}{k_1},\ \frac{H}{z}) \qquad (1)$$

If the scale ratio λ is

$$\lambda = \frac{L_p}{L_m}$$

where L is a characteristic length and subscripts m and p denote model and prototype, respectively, the models may be scaled if

$$t_p = \lambda\ t_m$$

and

$$A_p = \lambda\ A_m$$

---

[1] Variables are defined where they first appear and are arranged in a glossary in the Appendix.

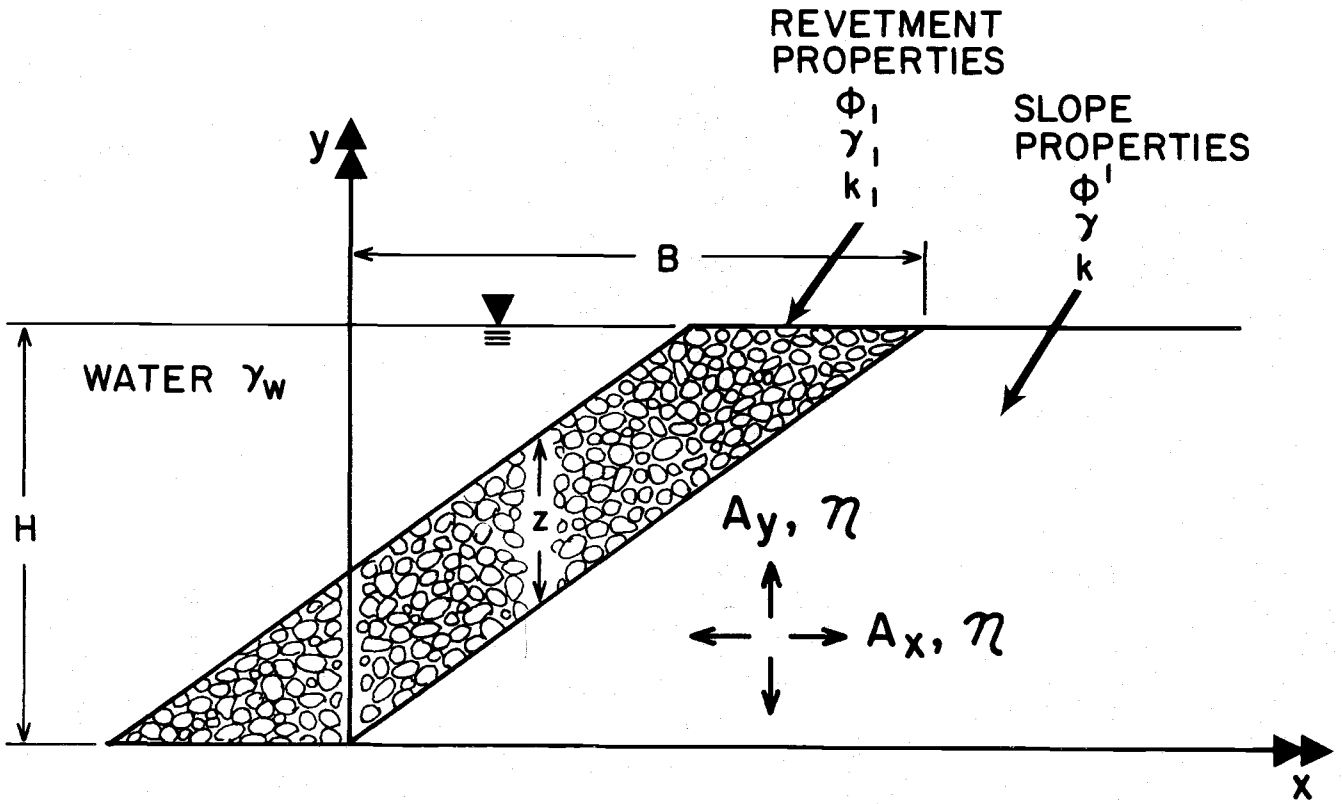

Figure 4a. Variables determining slope properties.

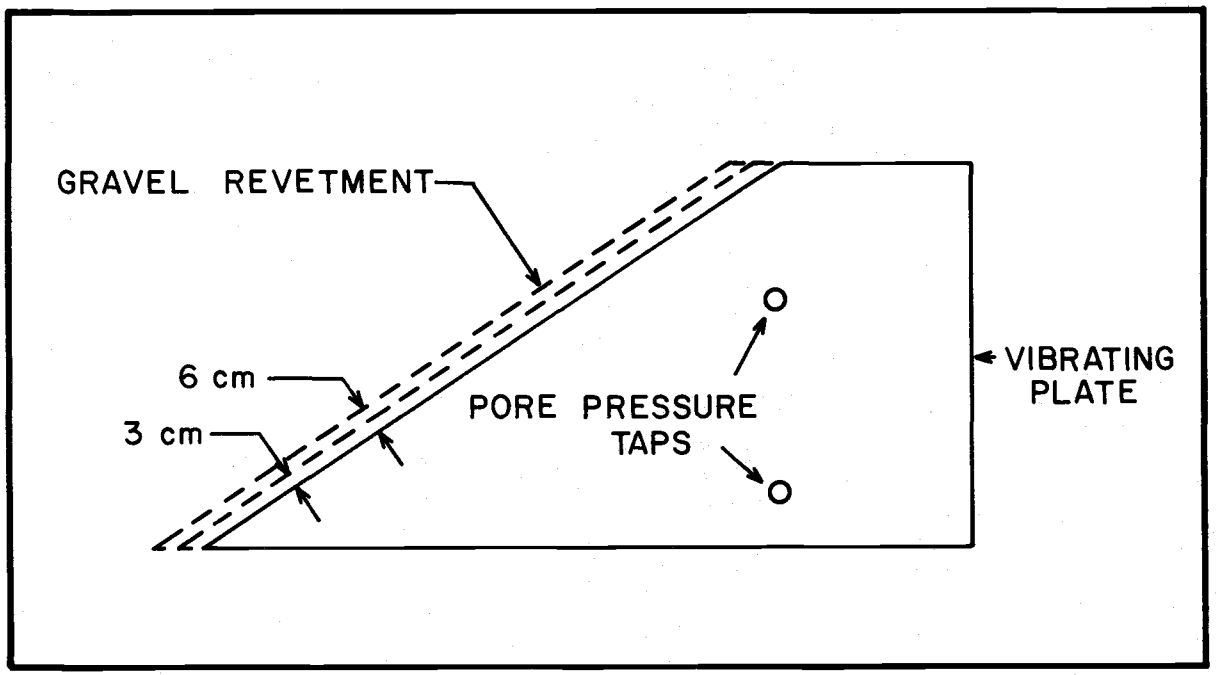

Figure 4b. Revetment thickness used on slopes.

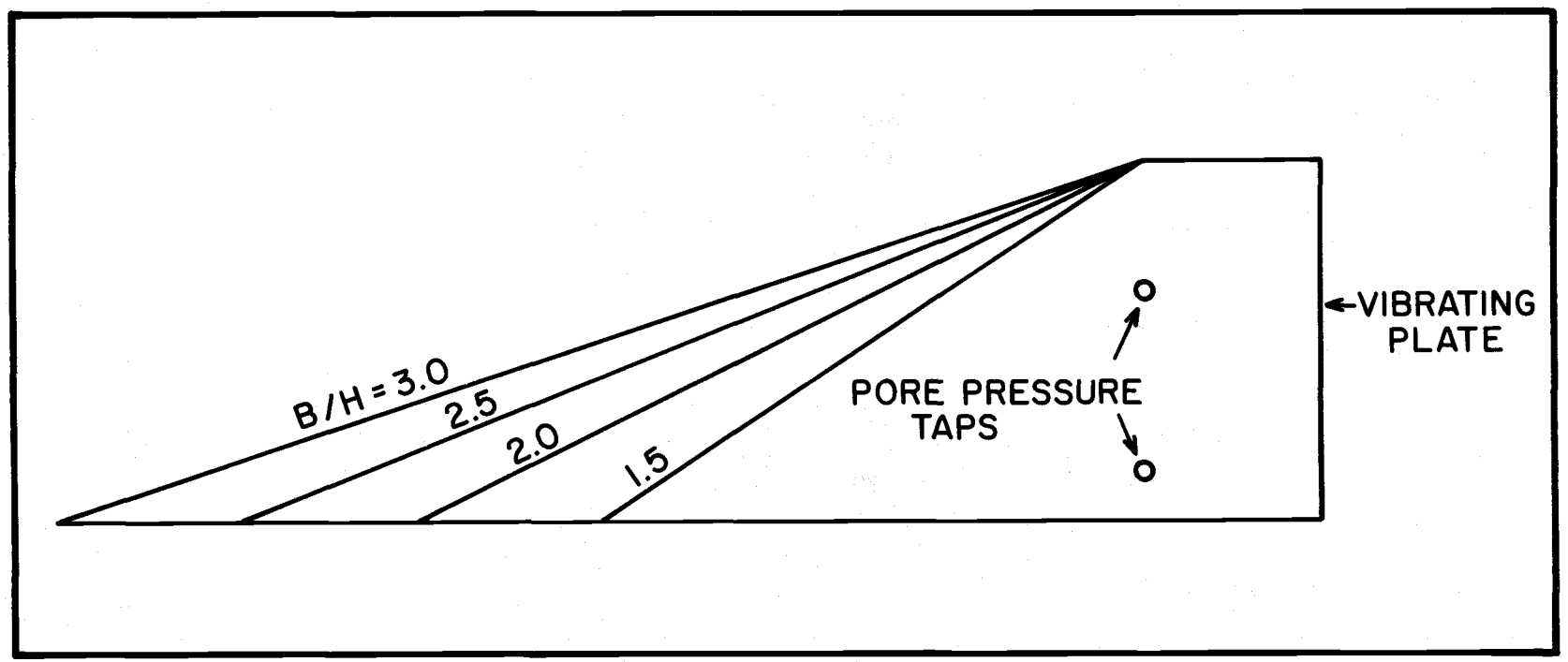

Figure 4c. Variations of slope angle.

provided the materials in model and prototype are the same. Three different size models were tested in order to determine the functional relationship among the dimensionless parameters shown in equation (1). Geometrically similar slopes of 40, 80 and 100 cm in height were subjected to internal vibration and the resulting increases in pore water pressure and final slope deformation were recorded. These responses were used to indicate the degree of instability produced in the slope. For all tests γ_w, γ, γ_1, ϕ', ϕ_1, k, and k_1 were assumed to be constant. The other parameters varied for each slope height as follows:

1) $\frac{B}{H}$ took on four values for each slope height, 1.5, 2.0, 2.5, and 3.0;
2) A and η were constant for a given slope height; and
3) The gravel thickness, z, had values of 0, 3, and 6 cm for each value of $\frac{B}{H}$.

These concepts are illustrated in Figure 4a, b, and c.

Apparatus and Procedure

The basic apparatus and procedures were designed to accomplish six general functions:

1) To build slopes and to transport the sand and gravel materials needed.

2) To monitor the assumption of uniform constant density for all tests.

3) To vibrate the slope, causing failure due to liquefaction.

4) To monitor and record the production of pore water pressure with time.

5) To monitor and record the acceleration and frequency of the vibration source.

6) To measure and record final slope deformations.

The sand used in this study was a uniform medium fine Columbia River sand. The grain size distribution for this material is shown in Figure 5. The gravel used was from the Willamette River. The gravel was rounded and ranged in size between 1/4 inch and 1 inch.

The equipment used to build slopes included a flume or tank, a slope face plate, and a jet pump and associated plumbing. A diagram of this equipment is shown in Figure 6. The tank was constructed with steel and plexiglas sidewalls and resembled a flume on the end where the slopes were formed. The other end of the tank was deeper and served as a holding basin for the sand used to form the slopes. The flume end of the tank was 4 feet deep and 2 feet wide. The plexiglas sidewalls aided in viewing the slope deformation during failure and were marked with a grid for making slope deformation measurements.

The combined water pump and plumbing system transferred the sand from the holding basin to the flume end of the tank in the form of

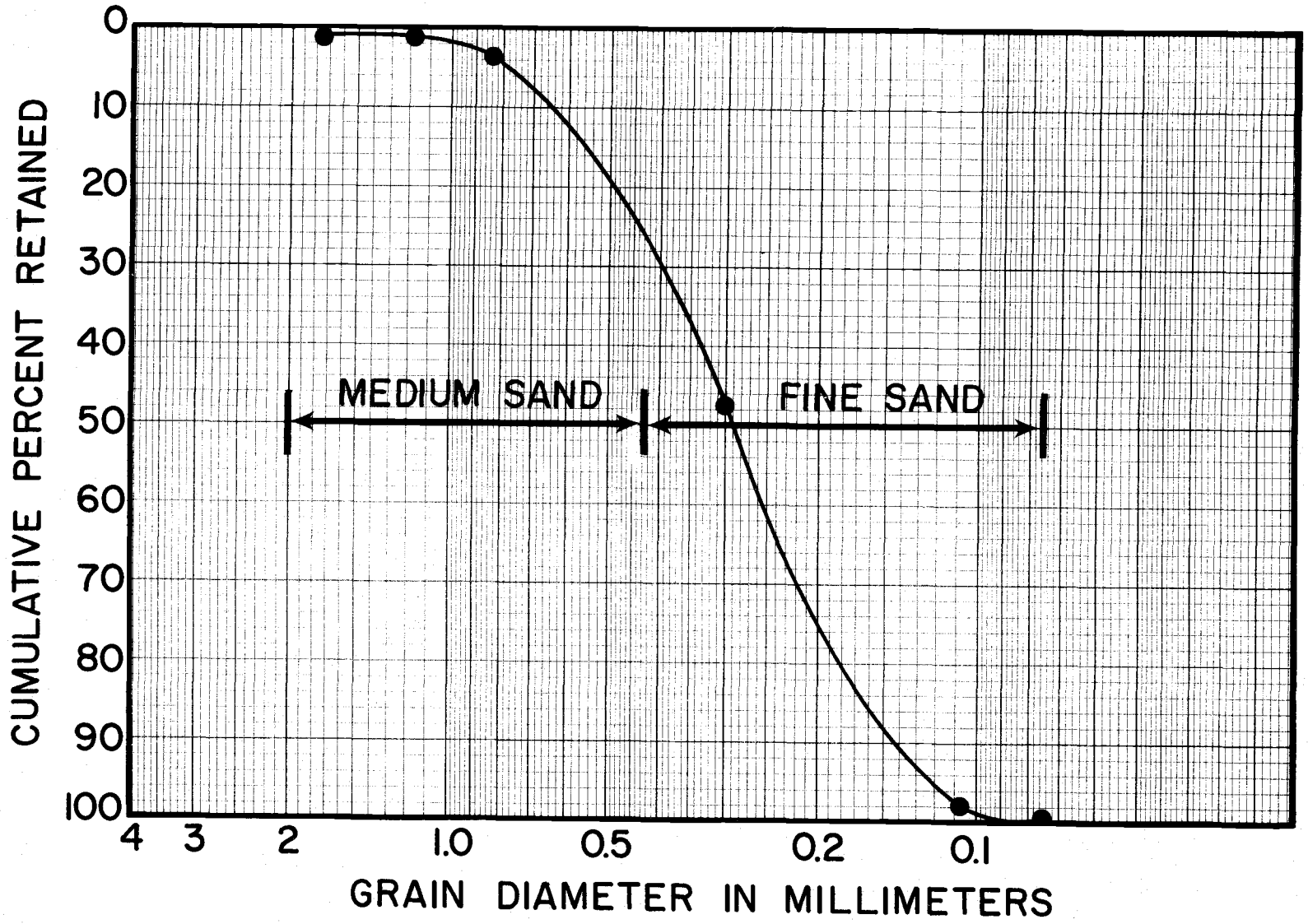

Figure 5. Grain size curve - Columbia River sand.

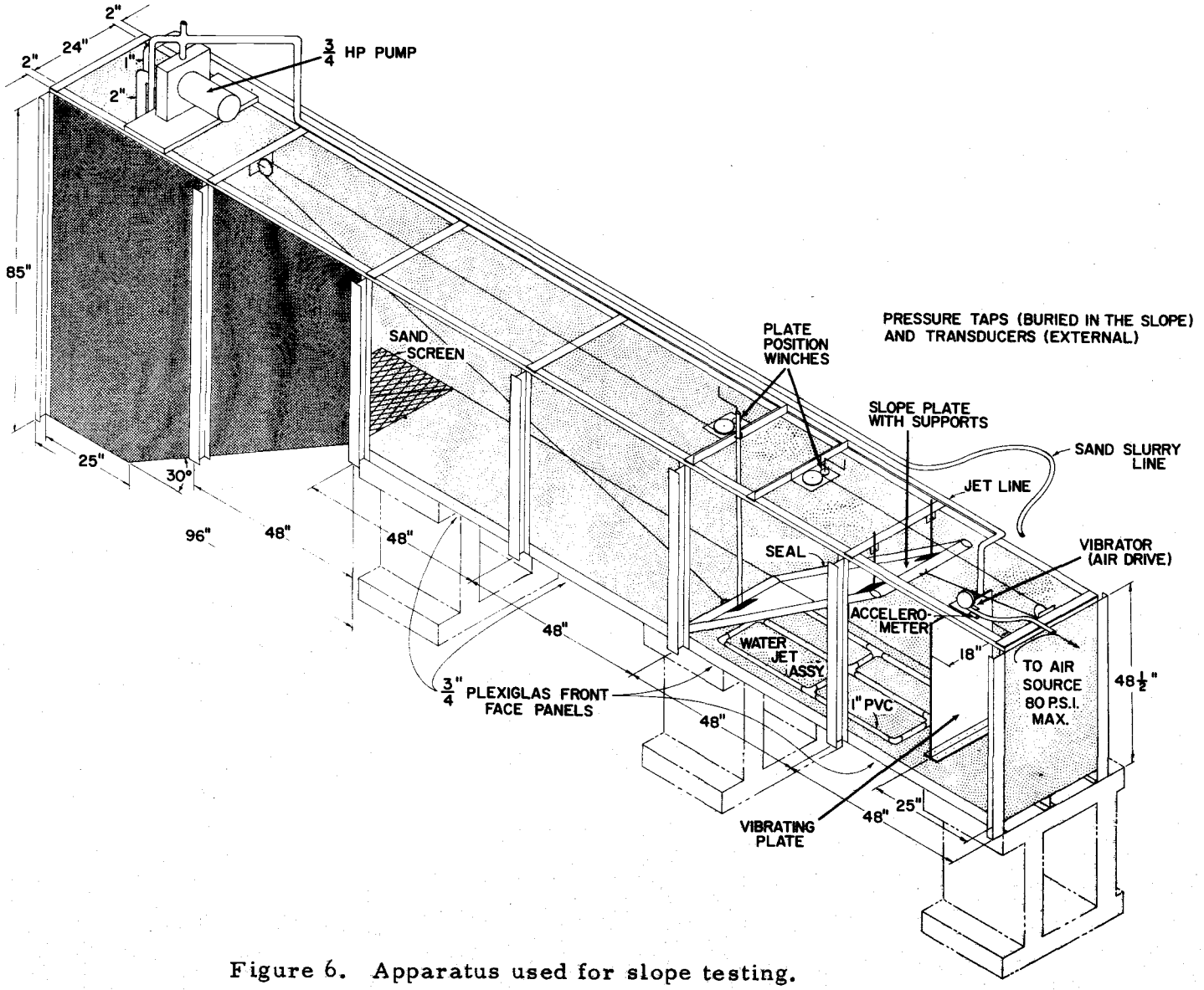

Figure 6. Apparatus used for slope testing.

a sand-water slurry. Water flowing through a jet pump in the bottom of the holding basin sucked sand into the line and deposited the slurry at the other end of the tank. The water pump was also arranged to pump water through another part of the plumbing system which was used to create a quick condition in the slope. A grid of perforated pipes was located on the tank bottom beneath the slope as shown in Figure 6. When water was pumped through the perforated pipe, the flow through the holes exceeded the critical gradient and loosened the sand.

When building an actual slope the slope face plate was bolted into position as shown in Figure 6. The plate could be adjusted for different slope angles and once in place, it formed a bulkhead which sealed against the sidewall of the tank as compressed air was forced into the bicycle inner tube rimming the outer edges. Since dense compacted sand was usually present from a previous test, it had to be loosened before more sand could be added. The sand was loosened by pumping water through the perforated pipes. Once the sand was loose, the jets were turned off and the sand slurry was pumped in behind the face plate until a complete slope had been formed. Both the loosening of the slope and the hydraulic placement of the sand were used in order to achieve a loose and uniformly dense deposit. Once the slope was formed, extreme care was taken to avoid jarring the tank and causing compaction of the loose sand. After the slope had been formed, the

face plate was removed with care to prevent eddies from eroding the slope face. Afterwards, if the slope was to be failed with a revetment, the gravel was placed by hand to avoid disturbance. At this time a large screen was placed on the bottom of the tank at the toe of the slope. After the test the gravel was scraped into the screen with a hoe and removed with winches and ropes.

Determination of Density Profile

Before each slope was vibrated, a density profile was obtained in order to check the assumption of uniform constant density. To accomplish this, a cone penetration device was designed and constructed. The device consisted of a Dutch cone (Figure 7) with a projected bearing area of 10 cm^2, attached to a proving ring by a 4-foot-long, slender shaft. In operation, the cone assembly was connected to a lever arm which had been bolted to the tank. Pulling down on the lever arm forced the cone into the soil.

The entire assembly in operation is shown in Figure 8. The loading ring dial readings were recorded with depth and were converted to density values using the calibration curve shown in Figure 9.

The calibration of the penetration apparatus was accomplished by forcing the cone into a container of saturated sand with a known dry density. The cone was pushed at a rate of 1 inch per minute and load readings were recorded for every 1/2 inch of penetration. Cone

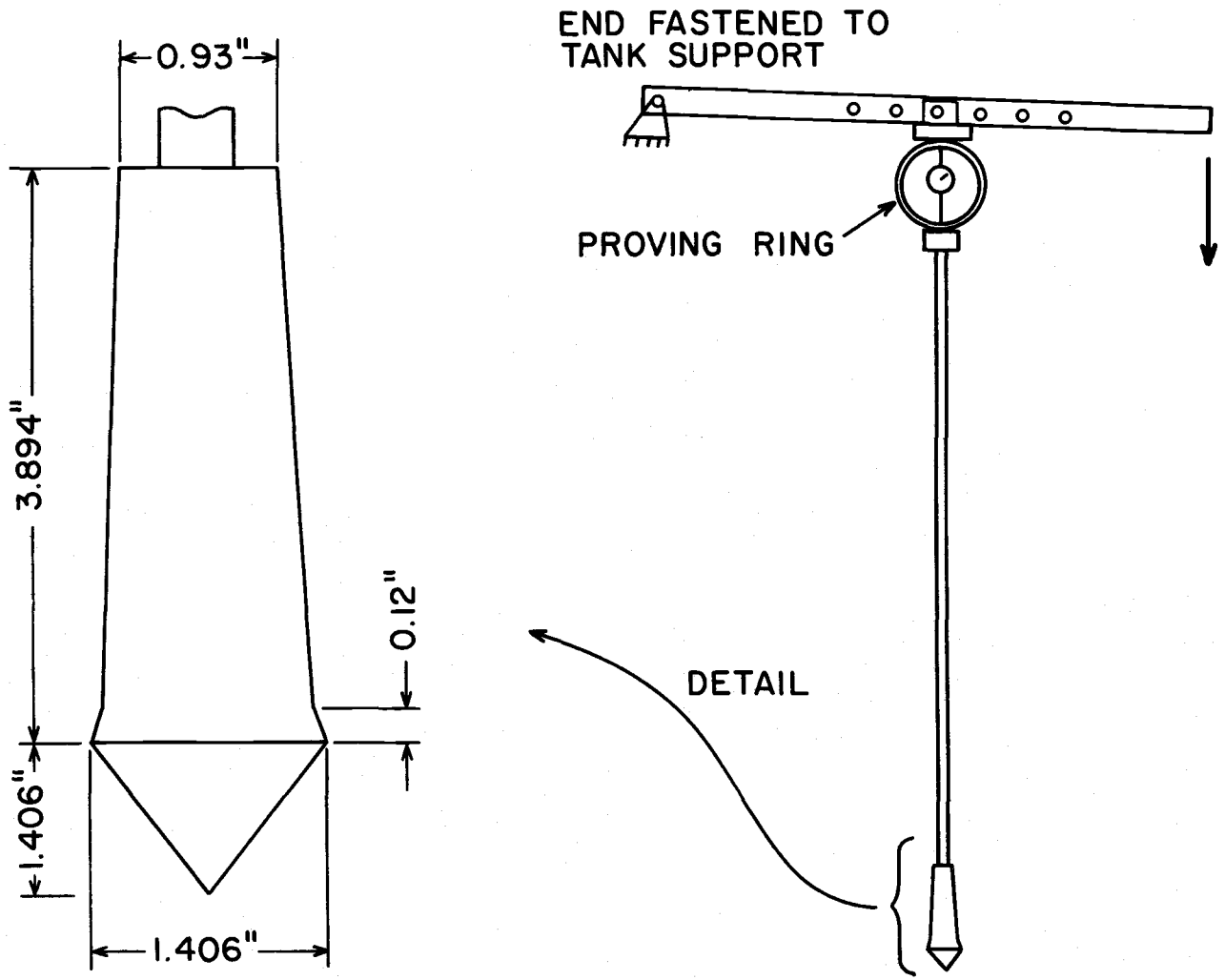

Figure 7. Dutch cone density apparatus.

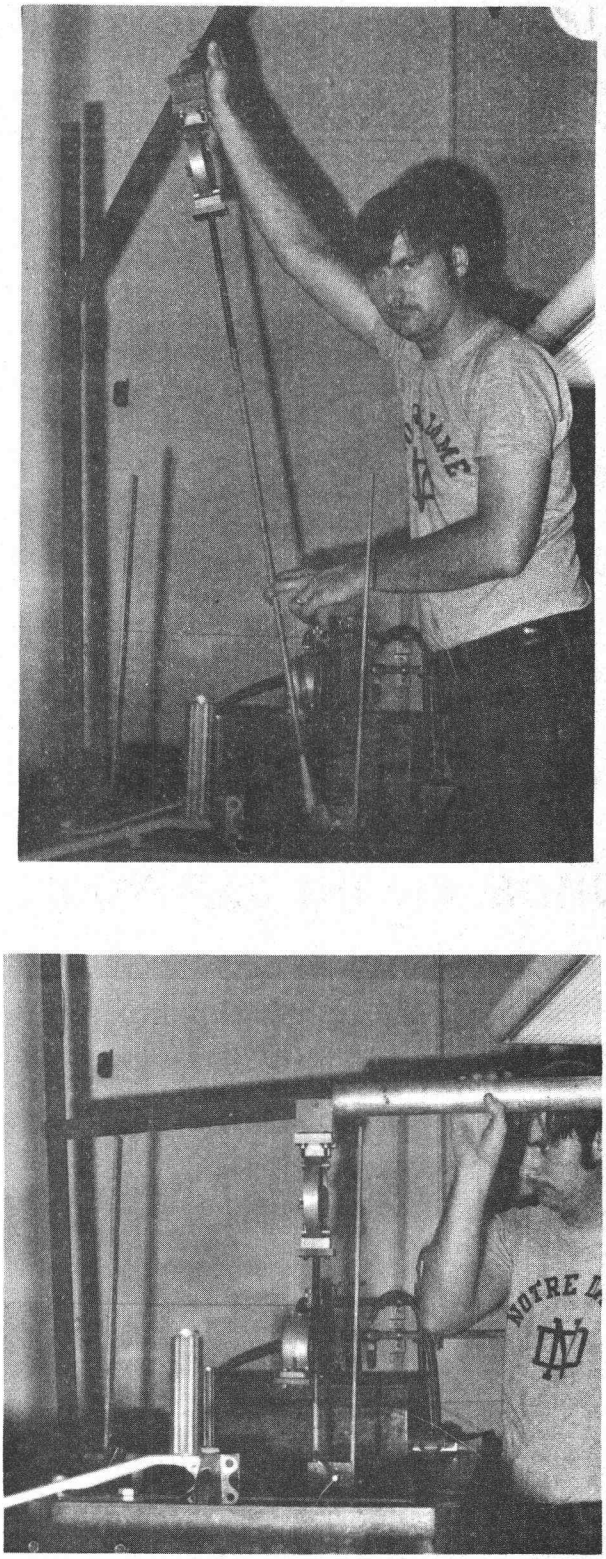

Figure 8. Dutch cone apparatus in use.

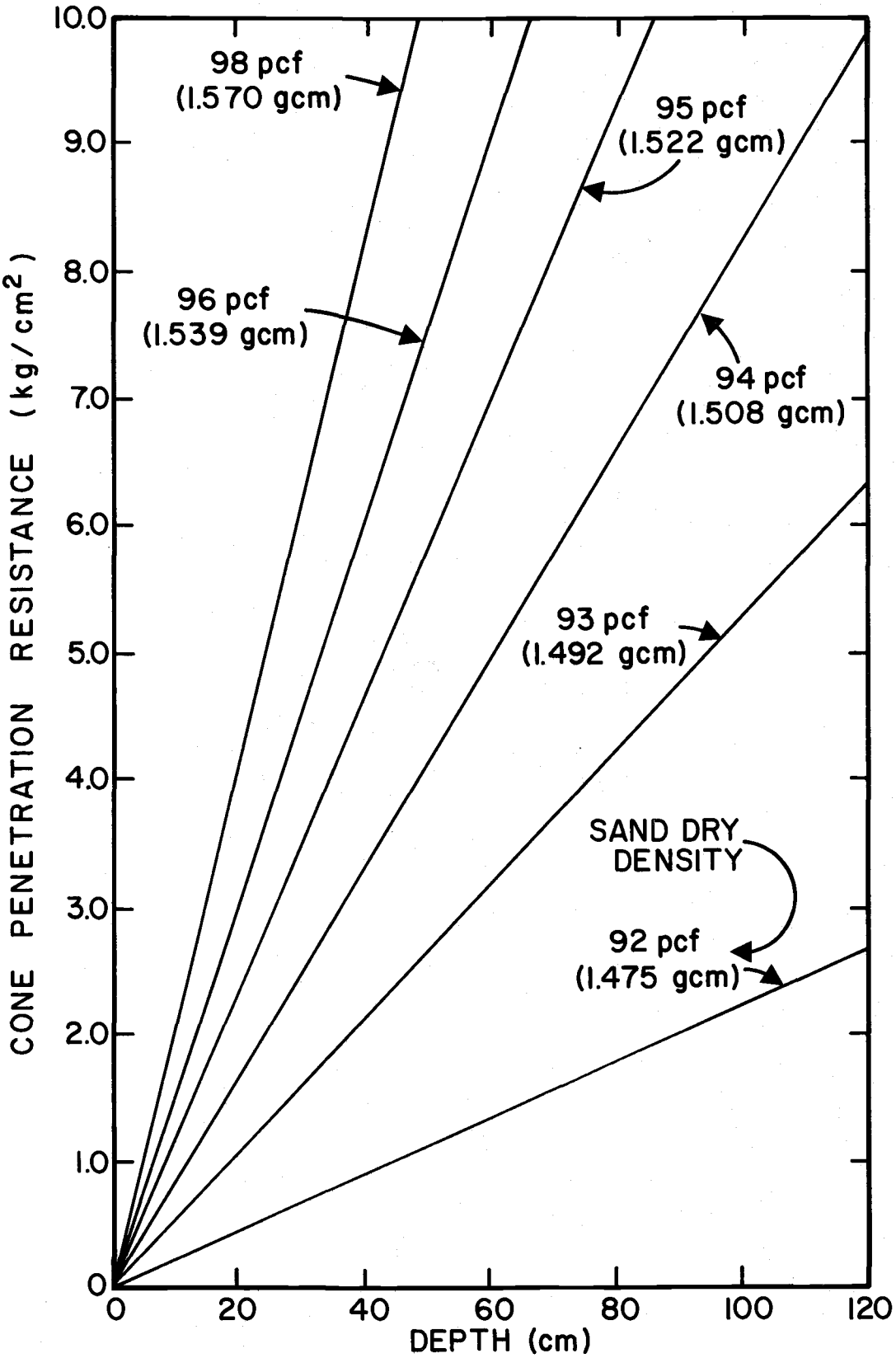

Figure 9. Density curve relating cone penetration and depth in deposit.

penetration resistance versus depth was then plotted for different values of dry density as shown in Figure 9.

The actual rate of penetration in the model slopes differed from the calibration conditions. The rate was increased to 6 inches per minute during slope testing when it became evident that several probes of the sample slope at different penetration rates provided almost identical results.

During calibration, efforts were also made to determine the effect of shaft resistance on the penetration resistance values. To eliminate shaft resistance required that the shaft be placed in a sleeve which could push the cone to the desired depth; the sand would then offer no resistance to the middle shaft as it and the cone were pushed to measure penetration resistance at that depth. Tests with and without the sleeve showed that shaft resistance was negligible. Therefore, the apparatus was used without the sleeve to simplify the pushing operation.

The actual testing of a slope involved vibrating it and recording the resulting pore water pressure increases and slope deformations. The vibration apparatus consisted of a 1/4-inch-thick piece of steel plate, 18 inches wide and 5 inches longer than the slope height. The plate was bolted to the bottom of the tank at the proper scale distance behind the slope crest for each slope height. The top of the plate was free to move. A compressed air actuated ball vibrator manufactured

by Cleveland Vibrator Company was mounted on top of the plate. A cross section of the plate and vibrator is shown in Figure 10. The steel ball in the vibrator rotated in the round, cylindrical chamber as shown, causing translation of the top of the plate. For all tests the air pressure was 75 psi, producing frequencies of vibration between 28 and 40 cycles per second depending on the plate length and embeddment. Acceleration of the top of the plate varied between 2 g and 6 g, also depending on slope height.

Data recorded during the tests included:

1) Pore water pressure with time for two locations in the slope, and
2) Horizontal acceleration of the top of the plate.

A pore water pressure measuring device consisted of a small diameter iron pipe piezometer tube connected with plastic tubing to a linear diaphragm-type strain transducer. A diagram of the pore pressure apparatus is shown in Figure 11. The strain transducer was a Statham UC3 compression-type with maximum load capability of 60 grams. A Statham UR5 regulated power supply provided power and signal readout for one transducer while a UR4 supplied power only to the other transducer. Both transducer signals were recorded on separate channels of a Honeywell 906c Visicorder oscillograph. The piezometer tubes were fastened through the steel back wall of the tank and projected into the center of the tank parallel to the bottom. The

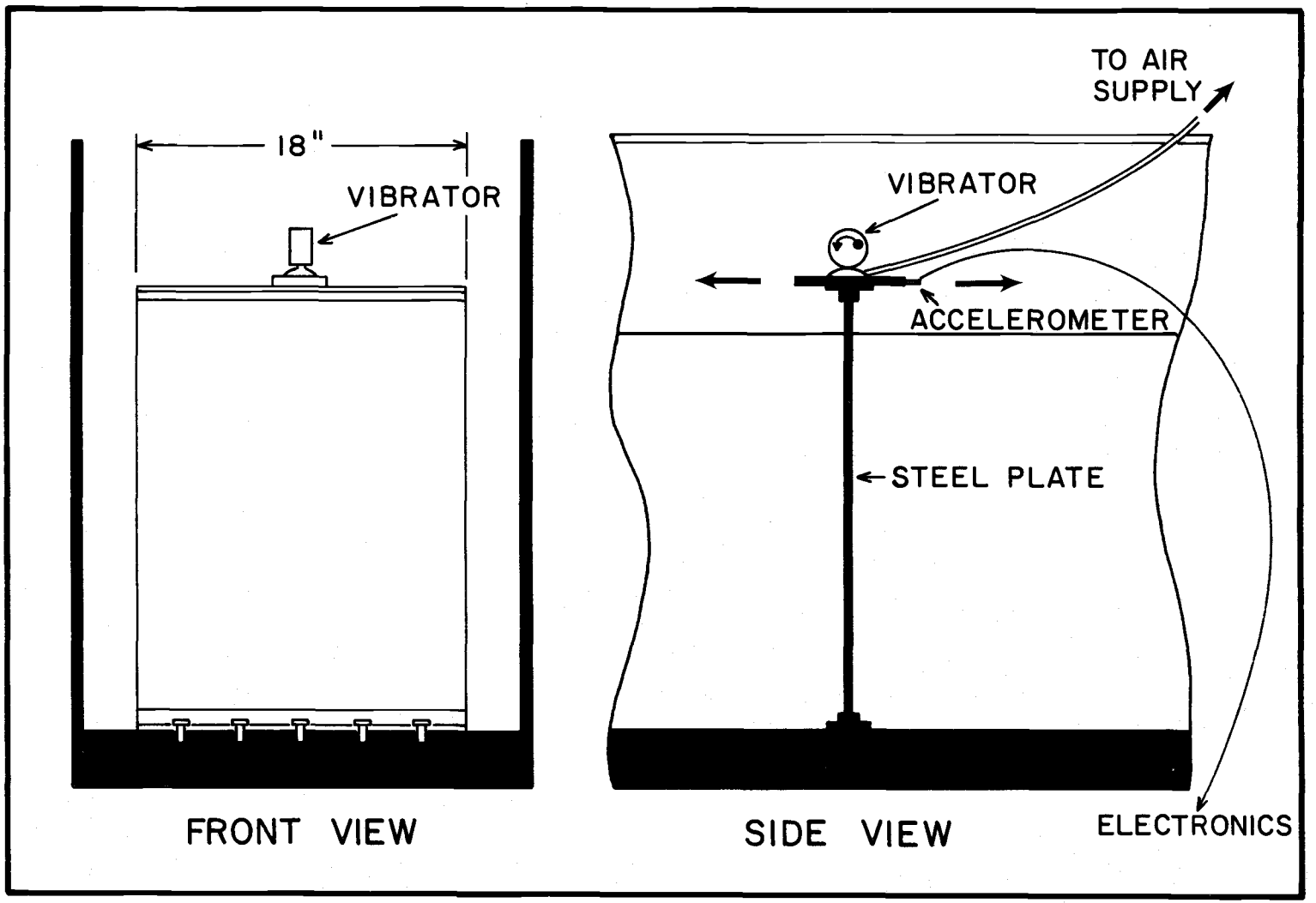

Figure 10. Excitation supplied by ball vibrator and steel plate.

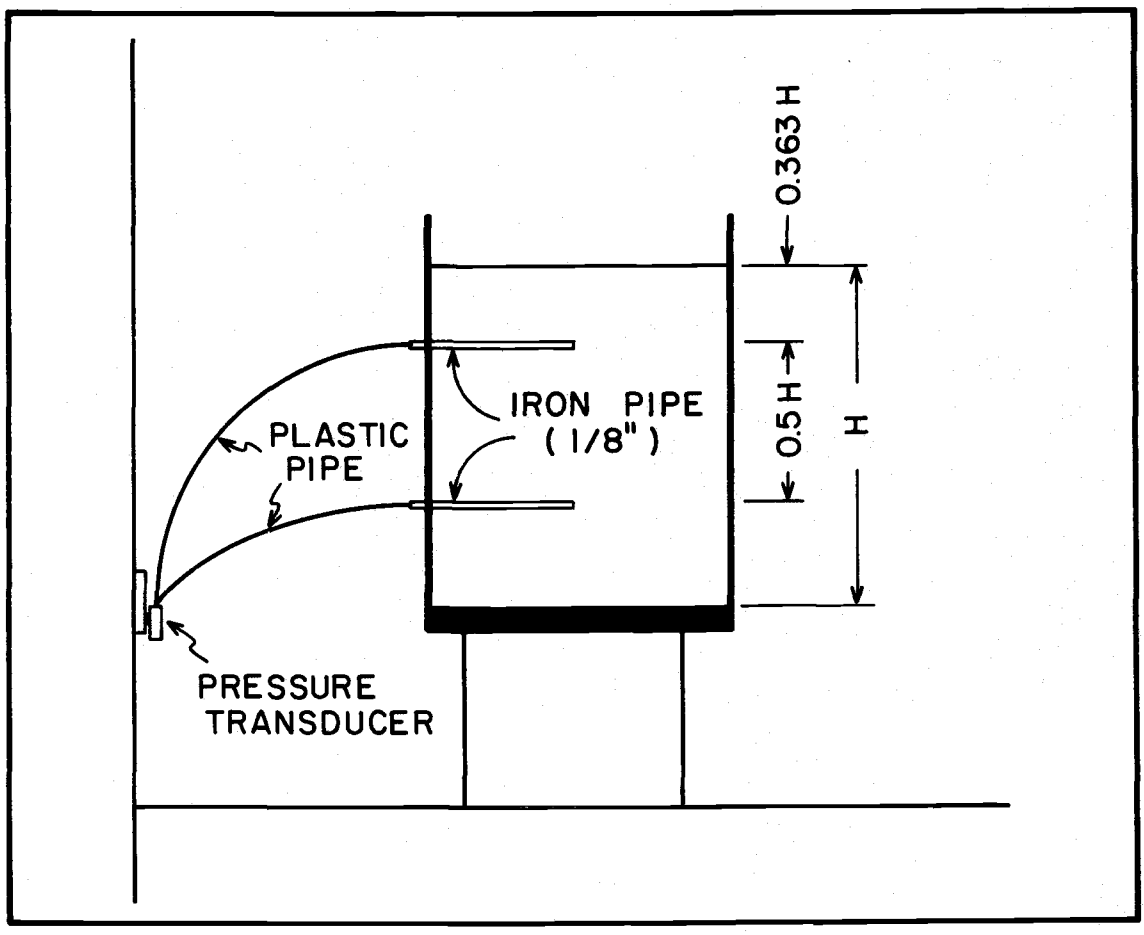

Figure 11. Tank cross section showing installation of pore pressure measuring devices.

tubes were located in the vertical cross section passing through the slope crest as shown in Figure 11. In the 80 cm slope the tubes were placed 29 and 69 cm from the top of the slope. The tubes were placed at corresponding scale distances for both the 40 and 100 cm high slopes.

Acceleration of the vibrating source was measured using a PCB quartz accelerometer Model 302A fastened to the base plate of the vibrating ball mechanism. The location of the accelerometer is shown in Figure 11. The acceleromter signal was also recorded on the 906c Visicorder.

Other data recorded included the final vertical deflection of the slope crest, the height of the free water surface above the piezometers, and the final shape of the deflected slope face. This information was obtained using a meter stick and the grid on the plexiglas side of the tank.

V. RESULTS AND DISCUSSION

The results of tests on 38 submerged sand slopes include both observational and quantitative data. During each test the pore pressure response of the sand and acceleration of the vibrating plate were recorded on the oscillograph. The final deformed shape of the slope was sketched. Each slope was observed during shaking to determine distinctive movements or ascertain failure modes. The vertical deflection of the slope crest and the pore pressure data were used to formulate the stability factors previously derived. These were then plotted against the dimensionless parameters describing the slope geometry. Those plots were used to investigate the validity of the scale model approach, while the observational data provided some interesting information on the various mechanisms of failure. Observations of slope movements proved particularly useful in trying to develop an explanation of some of the trends in the pore pressure data.

These results can best be discussed by considering two distinct categories of information. These categories include the study of failure modes as described by the observational data and the examination of the deformation and pore pressure response as criteria for description of stability.

Failure Modes

A failure mode is defined for purposes of this paper as the characteristic movement of a model slope in response to vibration. In general, three types of slope behavior were observed, with some minor variations. The generation of the three types of behavior varied with slope angle and revetment thickness. Differing density profiles produced minor changes in the typical behavior for a few tests. Hereafter, the three types of behavior shall be referred to as Type I, Type II, and Type III. In general, a Type I movement was characterized by a flow of slope material down the face of the slope along a plane parallel to the face. Type II behavior resulted in a limited flow which did not rupture the revetment. Type III behavior represented a stabilized condition whereby essentially no horizontal movement took place in the slope, even though liquefaction occurred in the sand.

Type I behavior was a flow slide caused by a combination of the sliding of the slope face material due to a decrease in the factor of safety against sliding, and a general liquefaction flow from the top of the embankment. Table 1 indicates the combination of revetment thickness, slope height, and slope angle for which a Type I flow occurred. It is apparent from the table that both revetted and non-revetted slopes suffered flow slide failures. In non-revetted slopes

Table 1. Failure modes which occurred for various combinations of slope height, slope angle, and revetment thickness.

H (cm)	B/H	z = 0 (cm)	3 (cm)	6 (cm)
40	1.5	I	I	III
	2.0	I	I	III
	2.5	I	II	III
	3.0	I	II	III
80	1.5	I	I	II
	2.0	I	I	III
	2.5	I	I	III
	3.0	I	II	III
100	1.5	I	I	III
	2.0	I	III	III
	2.5	III	III	III
	3.0	III	III	III

Failure modes:

I = Type I
II = Type II
III = Type III

the first movement began almost instantaneously (within 1 second) with the initiation of shaking and was characterized by movement of a layer of sand about 1 cm thick which began to slide from the upper half of the slope toward the toe. The movement was the same in revetted slopes except that the 3-cm-thick layer of gravel also moved along with the thin layer of sand. The sliding of the gravel also started soon after shaking began.

It is believed that this initial sliding was not a liquefaction flow but merely a slide along a failure plane parallel to the slope face caused by a loss in shear strength. The loss in shear strength was probably caused by the immediate breakdown of the grain-to-grain contacts and a subsequent rise in the pore pressure resulting from vibration. It is unlikely that the initial sliding of the slope face material was caused by full liquefaction in which the effective stress became equal to zero. On the face of a relatively steep slope it was only required that the strength of the sand be reduced enough to allow the soil mass to slide along the failure plane, pulled by gravity forces. The fact that the slope face material began to slide initially in an intact mass and that the occurrence of this type of flow decreased as the slopes became less steep indicated that initially a gravity flow had taken place, caused by decreased effective stress on a plane of failure. Table 1 shows that as the slope cotangent, B/H, increases for slopes with 3 cm revetments, there is some minimum slope angle which should experience a Type I failure.

The second development of the Type I failure was a liquefaction or flow slide which began about 1-2 seconds after the initiation of shaking. In this study a flow slide is defined as the movement of a mass of sand which has become fluid as the result of the reduction of the effective stress to zero by sudden increase in pore pressure and limited initial drainage. A layer of the top of the embankment at least 4 cm thick appeared to become a viscous liquid and began to slide horizontally; eventually flowing down the slope face. Once the thick layer of fluid sand had moved down the slope face, very thin layers of sand continued to slide from the top of the slope in a manner similar to the progressive failures described in the Seward quake. Most movement was complete after about 10 seconds even though slight settlement of the slope due to densification continued after that time. The diagram of an unrevetted slope and a revetted slope are shown after a Type I failure in Figures 12 and 13.

A Type II failure was strictly a limited liquefaction flow. The physical dimensions of the slope for which these few failures occurred are shown in Table 1. The Type II failure was characterized by the movement of a rather thick layer of liquefied sand in a horizontal direction, which caused the revetment to deform slightly without complete rupture. After approximately 2 or 3 seconds of shaking, a layer as thick as 1/5 of the slope height appeared to become liquid and move horizontally, bulging the revetment. After about 6 seconds all

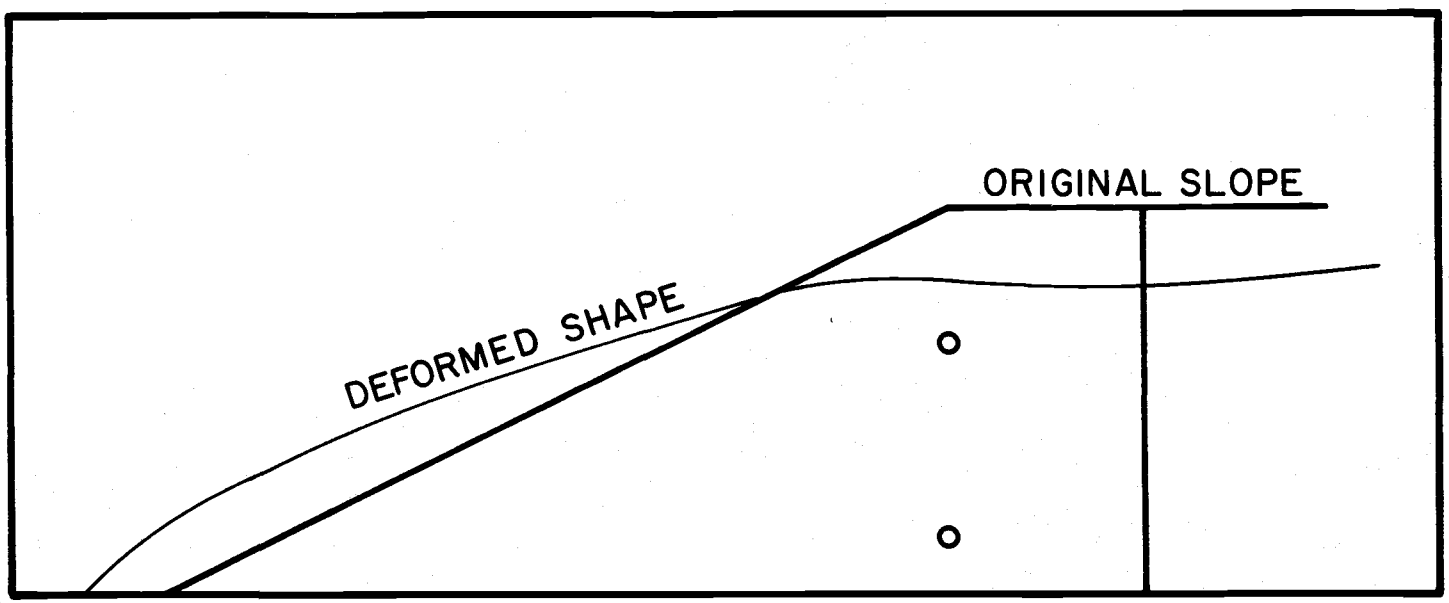

Figure 12. Failed slope diagram, Type I failure.

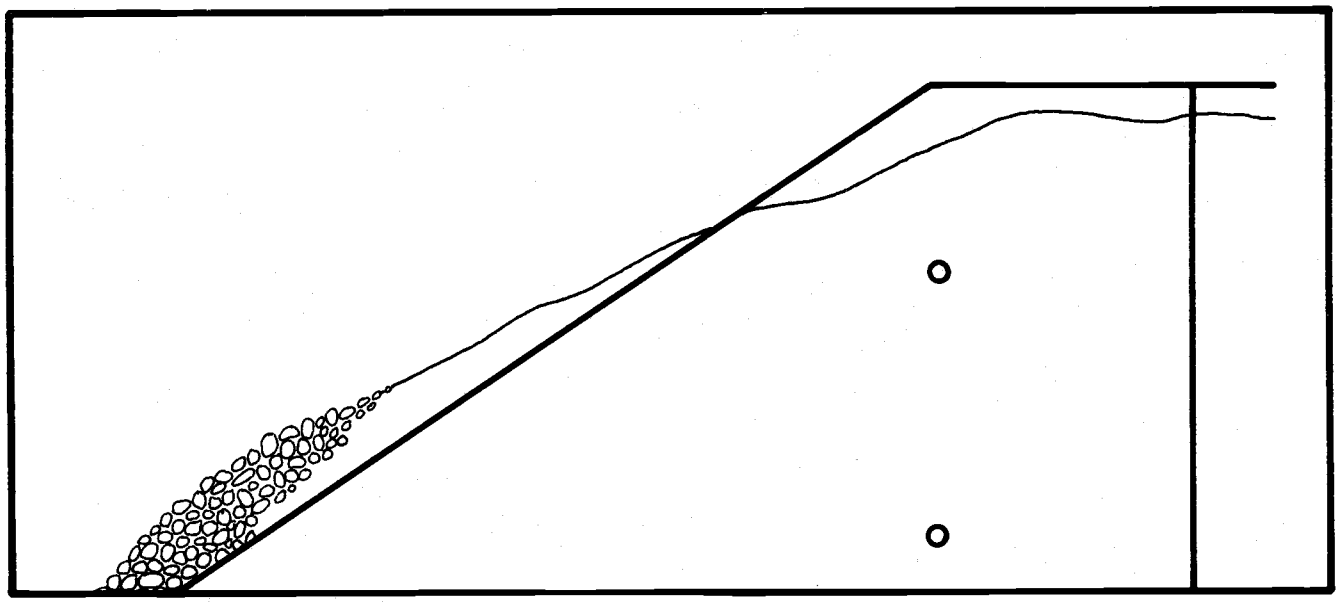

Figure 13. Failed slope diagram, Type I failure.

movement had ceased except for slight settlement due to densification. It was obvious that the sand had liquefied near the top of the slope even without referring to pore pressure records, since agitated sand particles could be seen moving around in a slurry while vigorous sand boils appeared in the top of the embankment in some slopes.

The Type II failure mode proved to be particularly interesting because it showed that a revetment could contain a flow slide and that a transition failure mode existed whereby a revetment could be used to prevent extensive flows, but which would result in limited deformation. The diagram for a typical slope which suffered a Type II failure is shown in Figure 14.

A Type III failure mode was not really a failure in the sense that a flow slide developed. In fact, slopes were completely stabilized against horizontal movement when this type of response occurred. As soon as shaking started in these tests the top of the embankment began to settle but the revetment did not move. In every case the top of the embankment liquefied to a depth of as much as .20H, while within the liquefied mass churning sand and water formed vigorous sand boils. A diagram of a typical slope after a Type III failure is shown in Figure 15 and indicates that the only movement of the entire embankment consisted of the settlement of the top. These failures showed that a large enough revetment could prevent all flow by acting as a barrier to retain the liquefied mass.

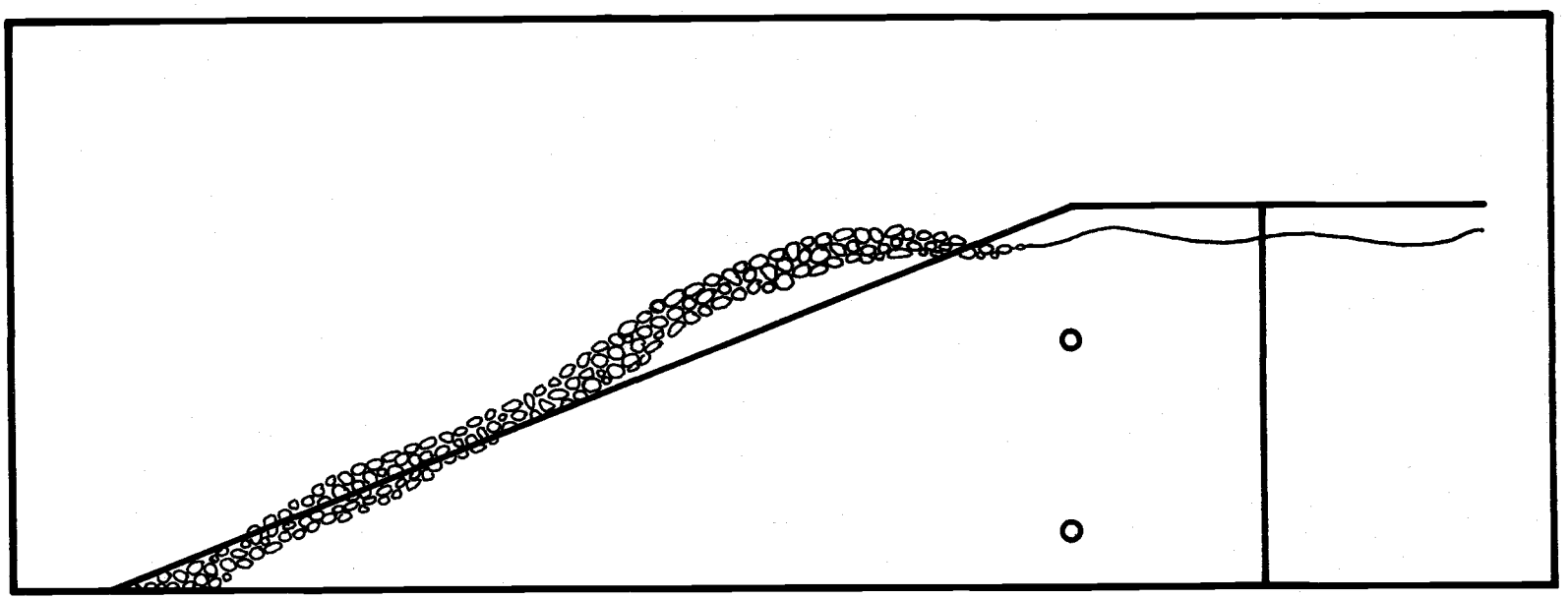

Figure 14. Failed slope diagram, Type II failure.

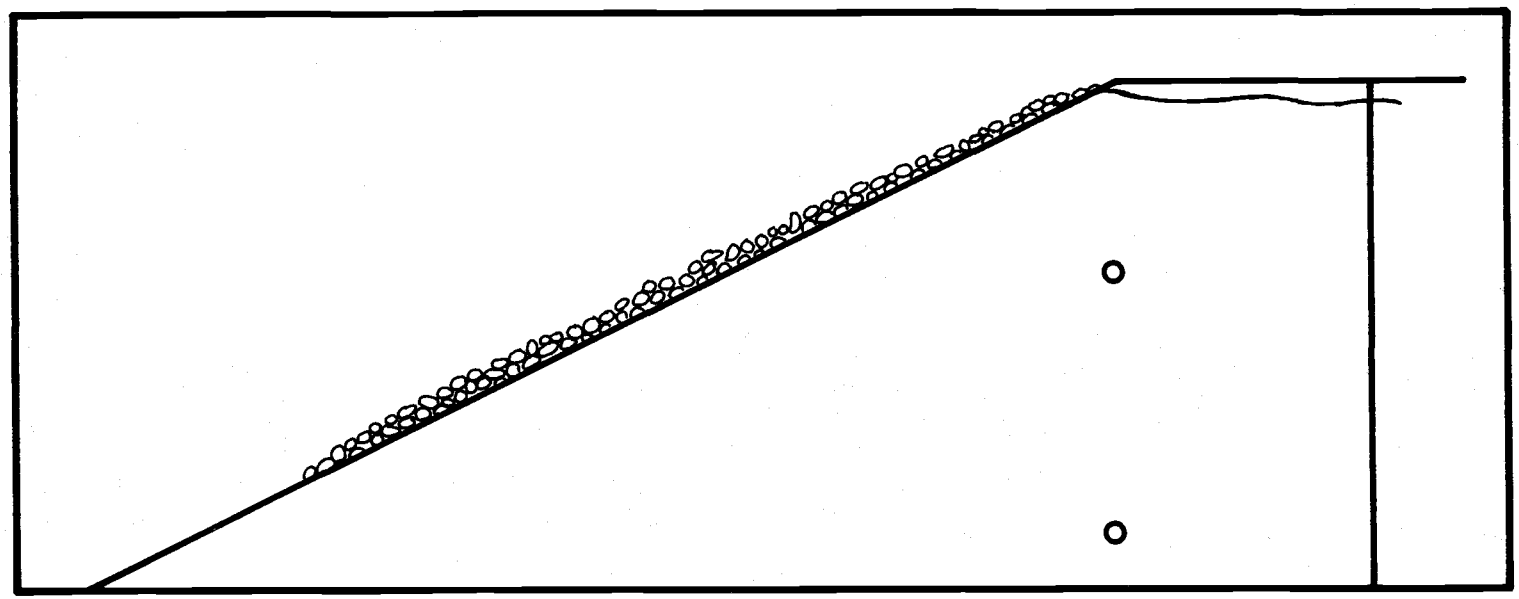

Figure 15. Failed slope diagram, Type III failure.

Effects of Density

It was expected that variations in density profile between different slopes could affect the occurrence of the three failure modes, and some effort was made to examine this possibility. Although it was our intent to insure that density would be constant for all the test slopes, it soon became apparent that this was a practical impossibility and that each slope had a different density profile. After testing several slopes with identical dimensions but differing density profiles, it was apparent that, although the pore pressure response of such slopes varied considerably, it was impossible to cause a change in failure mode within the range of density profiles for the tests. The only visual differences in these instances was that a denser slope resulted in a slightly slower and less dramatic pore pressure response. In a Type I flow, for example, when the sand was relatively dense throughout the slope, the movements already described required 1-2 seconds longer to occur and final deformations of the slope were somewhat smaller. In a Type II failure the depth of liquefaction and the final horizontal movement was not as large as the movement in a loose slope. For a Type III failure there were fewer sand boils and a smaller depth of liquefaction for dense slopes. It should be emphasized, however, that the term "dense slope" was a subjective description made by the writer. Although density

profiles were recorded for each slope using the Dutch cone apparatus, the resulting data could not be transformed into a single value describing the slope as dense or loose. Since every slope had dense and loose layers located in different positions the writer resorted to describing the slope as loose or dense based on the relative density of the top half of the slope. This seemed to work well for describing failure modes but did not work at all for relating the effects of density to pore pressure and deflection observations.

Deflection Criteria

The slope deflection was measured for each test and used in an attempt to find a stability function based on the dimensionless parameters describing the slope. The change in height of the slope measured at the crest was used to characterize the slope deflections. Figure 16 shows the stability parameter, dimensionless deformation ($\Delta H/H$), plotted against dimensionless revetment thickness for B/H values of 1.5, 2.0, 2.5, and 3.0. Delta H is the change in height of the slope crest and the other variables were defined in Figure 4. It can be seen from Figure 16 that the extreme scatter of the points eliminated any hope of developing a regular function for stability. However, it was interesting to note that all of the dimensionless deflection values for slopes that failed in particular mode could be grouped together. Figure 16 shows these values of $\Delta H/H$ grouped

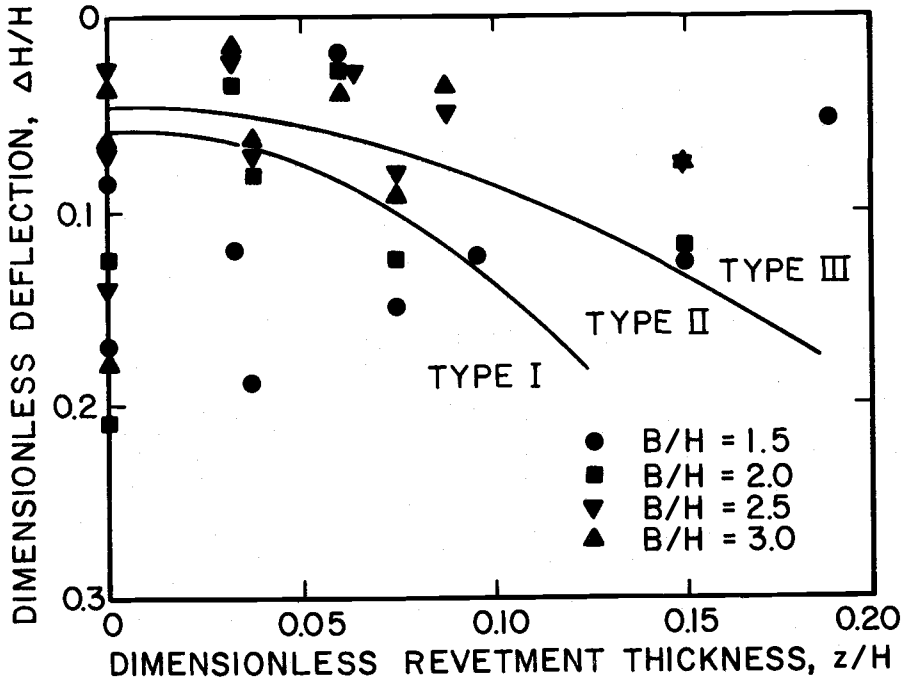

Figure 16. Deflection response of slope crest.

according to the type of failure. According to these results similar failure modes produced similar magnitudes of dimensionless deflection, with the largest deflections occurring for the combined gravity and liquefaction flow (Type I) and the smallest deflection occurring for the no flow (Type III) condition. As revetment thickness increased, the deflections generally were smaller for all slopes, which reflected the fact that increasing the revetment thickness caused the failure mode to change for all slopes.

The dimensional analysis of the sand slope model developed earlier showed that stability was a function of H/A and $k/H\eta$ as well as B/H and z/H. Since in Figure 16 the dimensionless deflection criteria was plotted only with B/H and z/H it was necessary to normalize values of ΔH by accounting for the scale relationship of acceleration and frequency and hope that the scatter in the data would be eliminated. The acceleration, A, and the frequency, η, were constant for a single value of slope height and therefore the relationship between stability and H/A and $k/H\eta$ for constant H was constant and linear. This requires that since

$$\text{Stability} = f(H/A,\ k/H\eta,\ z/H,\ B/H)$$

and

$$H/A \text{ and } k/H\eta = \text{constant} = C_1$$

for a single value of H then

$$\text{Stability} = C_1 f(z/H,\ B/H)$$

To normalize the stability data it was necessary to divide the stability values for a single H value by the constants representing the frequency and acceleration for that slope height:

$$\text{Normalized Stability} = \frac{\text{Stability}}{\text{Constant}} = f(z/H,\ B/H)$$

The deflection stability values were normalized in this manner but replotting the values showed that the scatter of the data was increased and no function of stability could be derived. An effort was then made to discover the possible effects of other parameters.

In the first place it became obvious as testing progressed that it was impossible to maintain a constant density profile for all of the slopes as was originally assumed. Although an attempt was made to quantify density and apply some correction factor to the deflection stability values, the density profiles of all the slopes were too non-uniform to describe with a single number. Thus, it seems likely that variations of density did effect the deflection results but it is impossible to determine what that effect was.

Secondly, even if acceleration, frequency and density were all accounted for, it is unlikely that a model relationship would exist for the stability of revetted slopes as measured by a dimensionless deflection, at least for the slopes in this study. The problem was that the deflections compared in Figure 16 were the result of three entirely different failure modes and it seems logical that deflection

can only be compared for slopes in which the mechanism of failure is similar. However, even after looking at the groups of data representing the various failure modes, no functional relationship for stability could be discerned and therefore it must be assumed that no relationship exists or that complex variations of parameters originally assumed constant have scattered the results.

Pore Pressure Criteria

The pore pressure change induced by vibration was measured at the points in the slope representing the scaled distance shown in Figure 11. The maximum pore pressure, u, was divided by σ_v, the total vertical pressure (computed assuming a level deposit) due to water and soil at the depth of the piezometer tap. This dimensionless pore pressure was then plotted against z/H for various values of B/H. The results of all the tests consist of u/σ_v plots for upper and lower piezometer taps and these results are shown in Figures 17a, b, c, d and 18a, b, c, d. The value of u/σ_v was an indication of the degree of liquefaction, with the maximum value of 1 indicating that the pore pressure equaled the total pressure, or that the effective stress was equal to 0 and that the sand had liquefied. It can be observed from the figures that some values of u/σ_v were slightly greater than one. This was probably due to small errors in instrument calibration. Since some of the pore pressure values for the 80 cm slopes were as

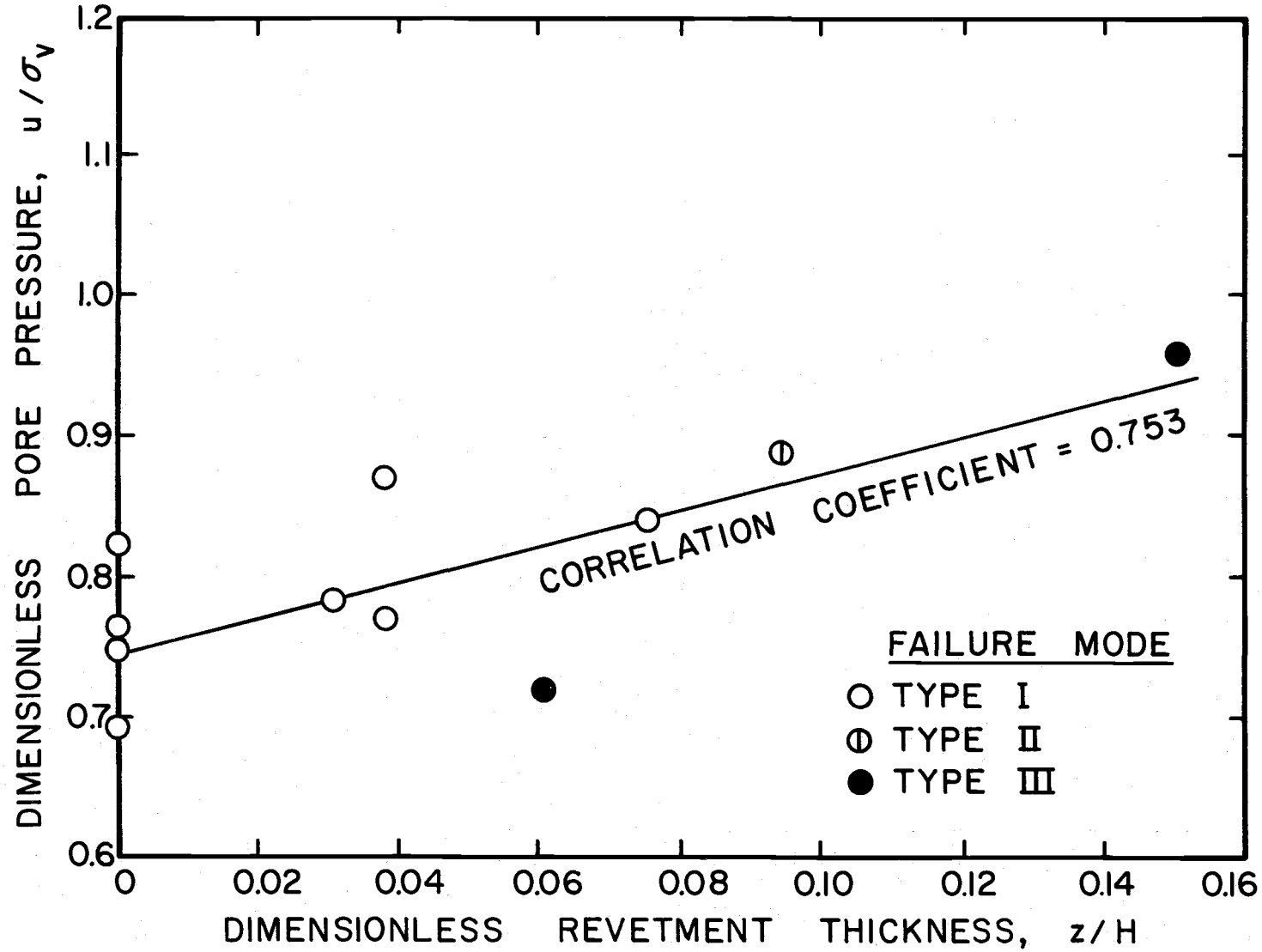

Figure 17a. Pore pressure response upper tap, B/H = 1.5.

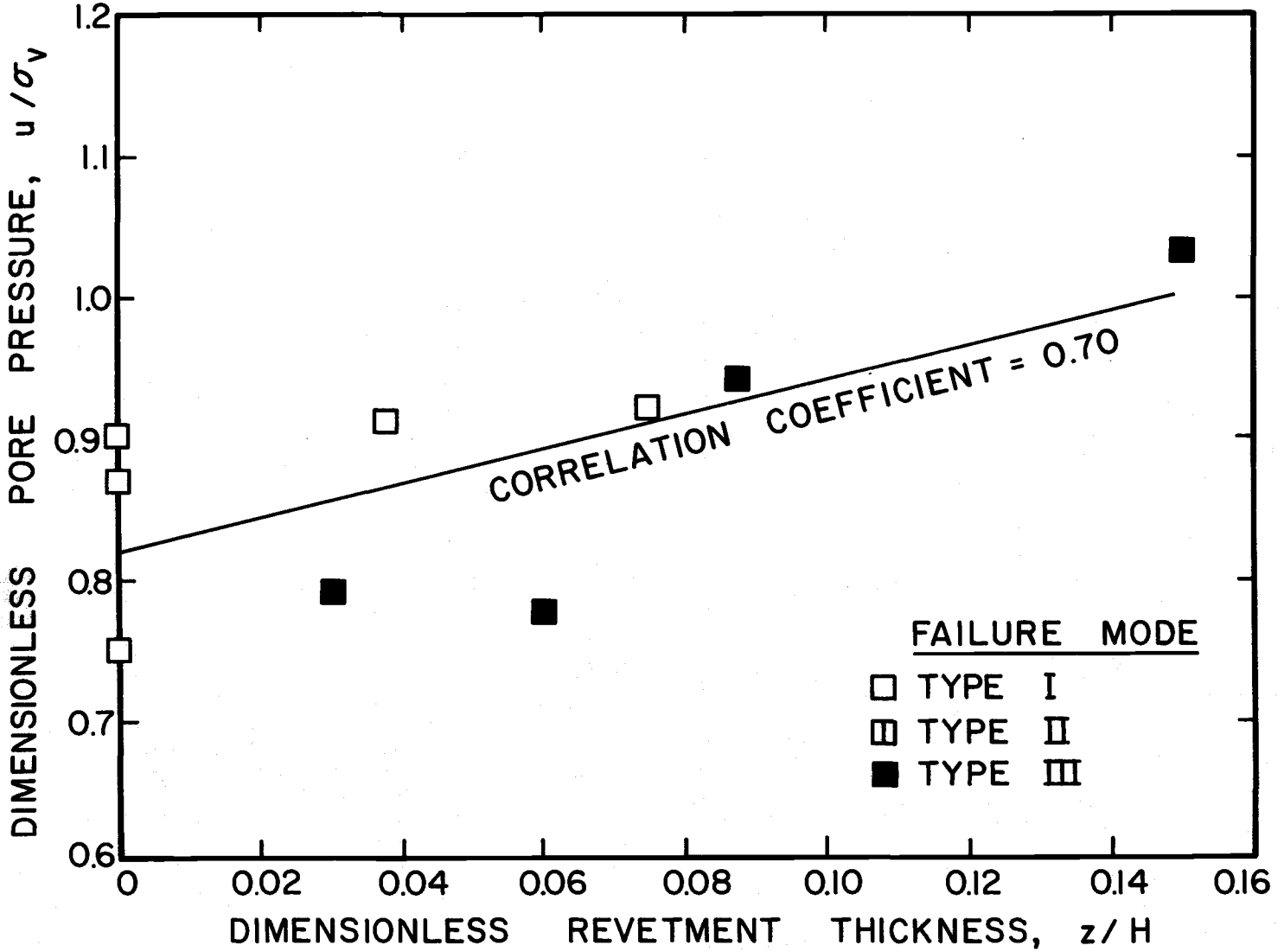

Figure 17b. Pore pressure response upper tap, B/H = 2.0.

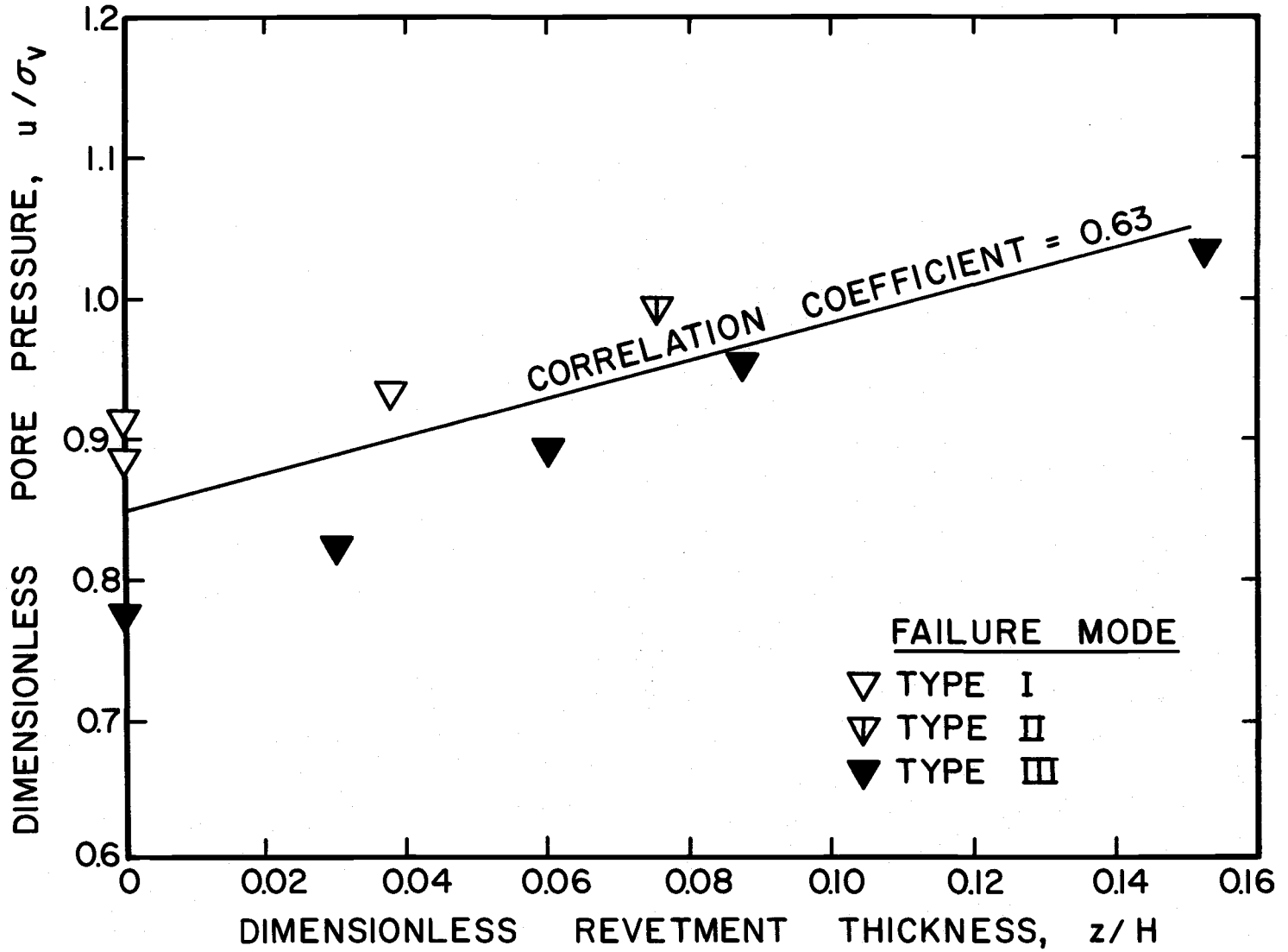

Figure 17c. Pore pressure response upper tap, B/H = 2.5.

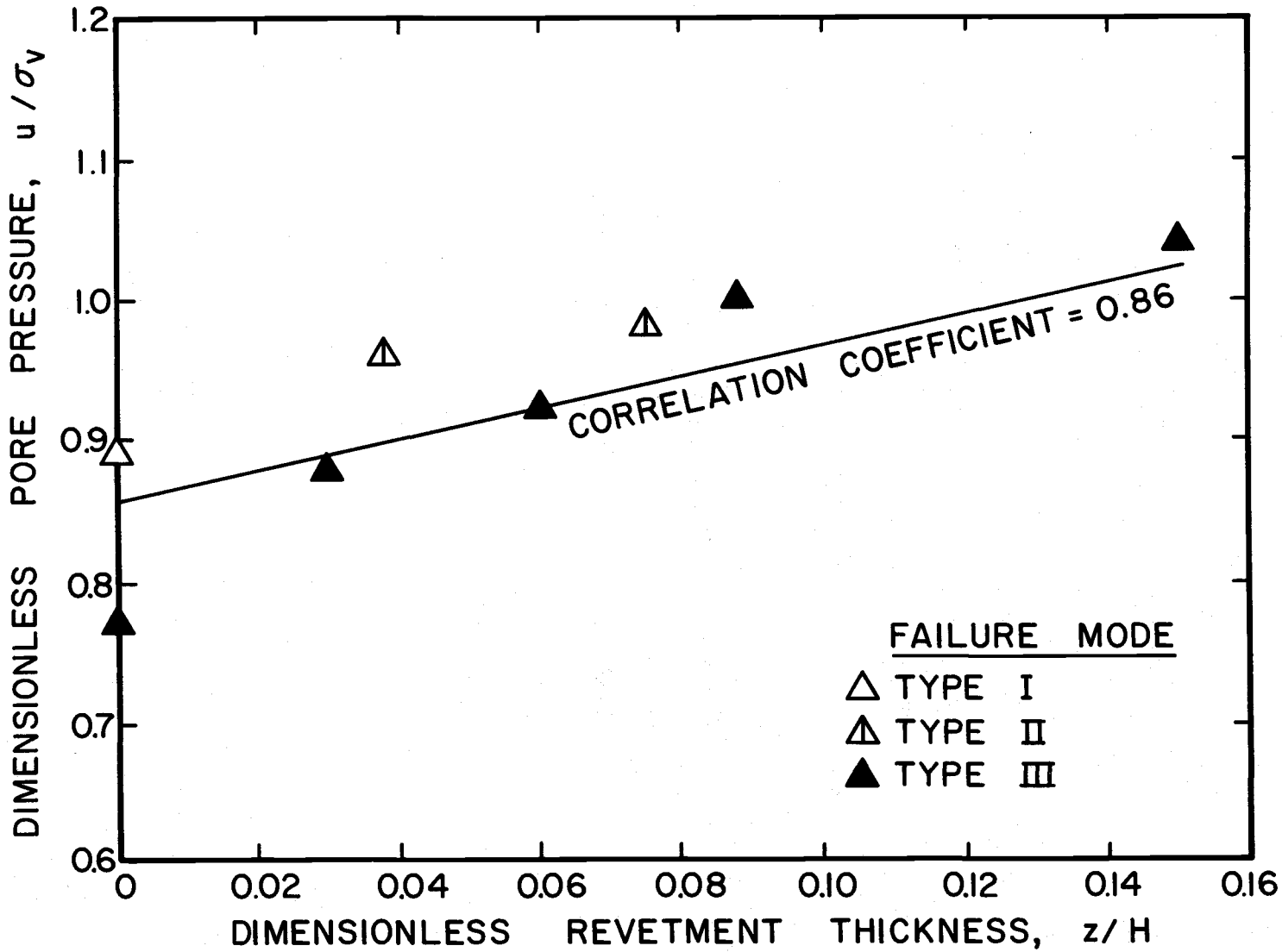

Figure 17d. Pore pressure response upper tap, B/H = 3.0.

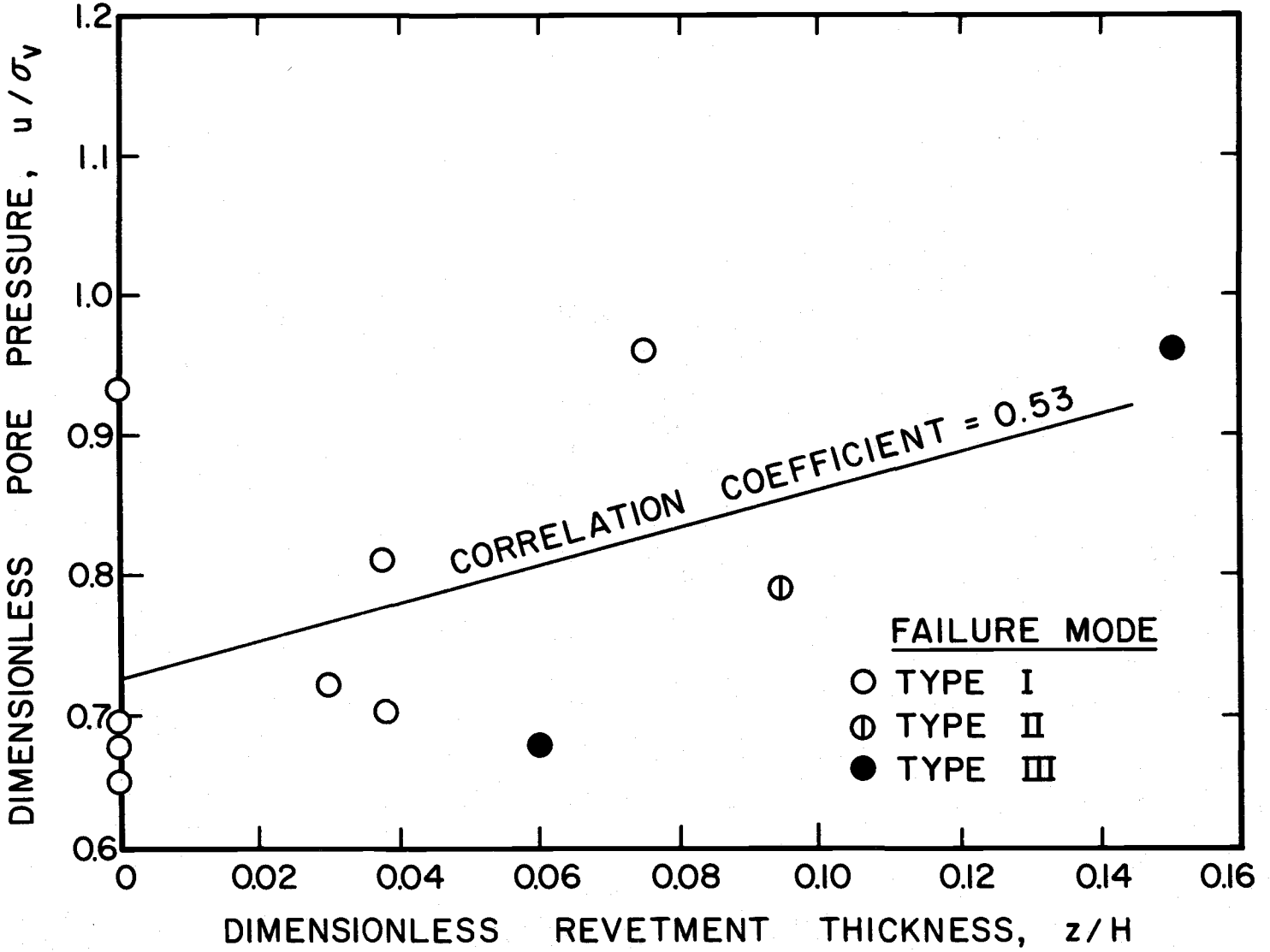

Figure 18a. Pore pressure response lower tap, B/H = 1.5.

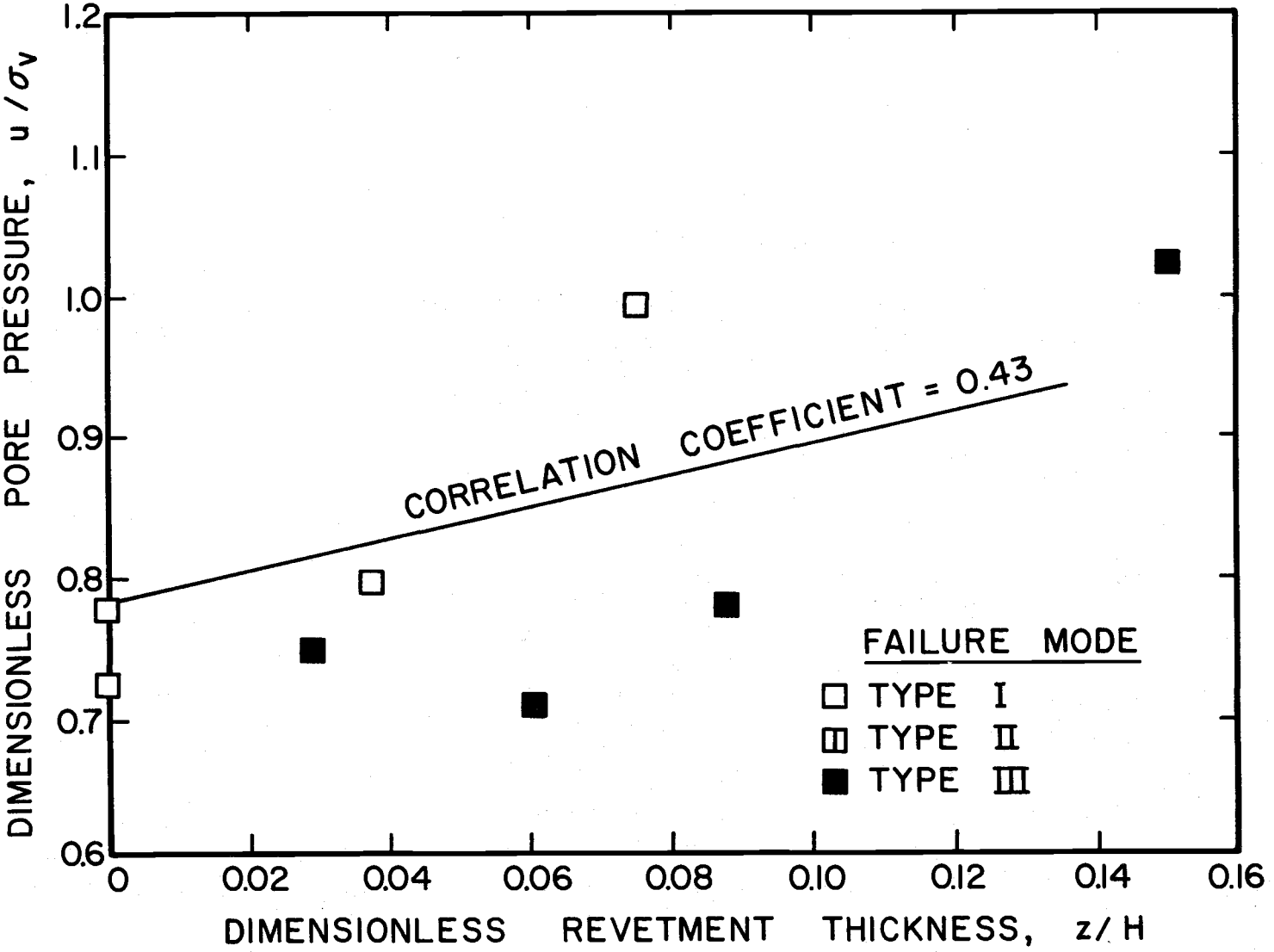

Figure 18b. Pore pressure response lower tap, B/H = 2.0.

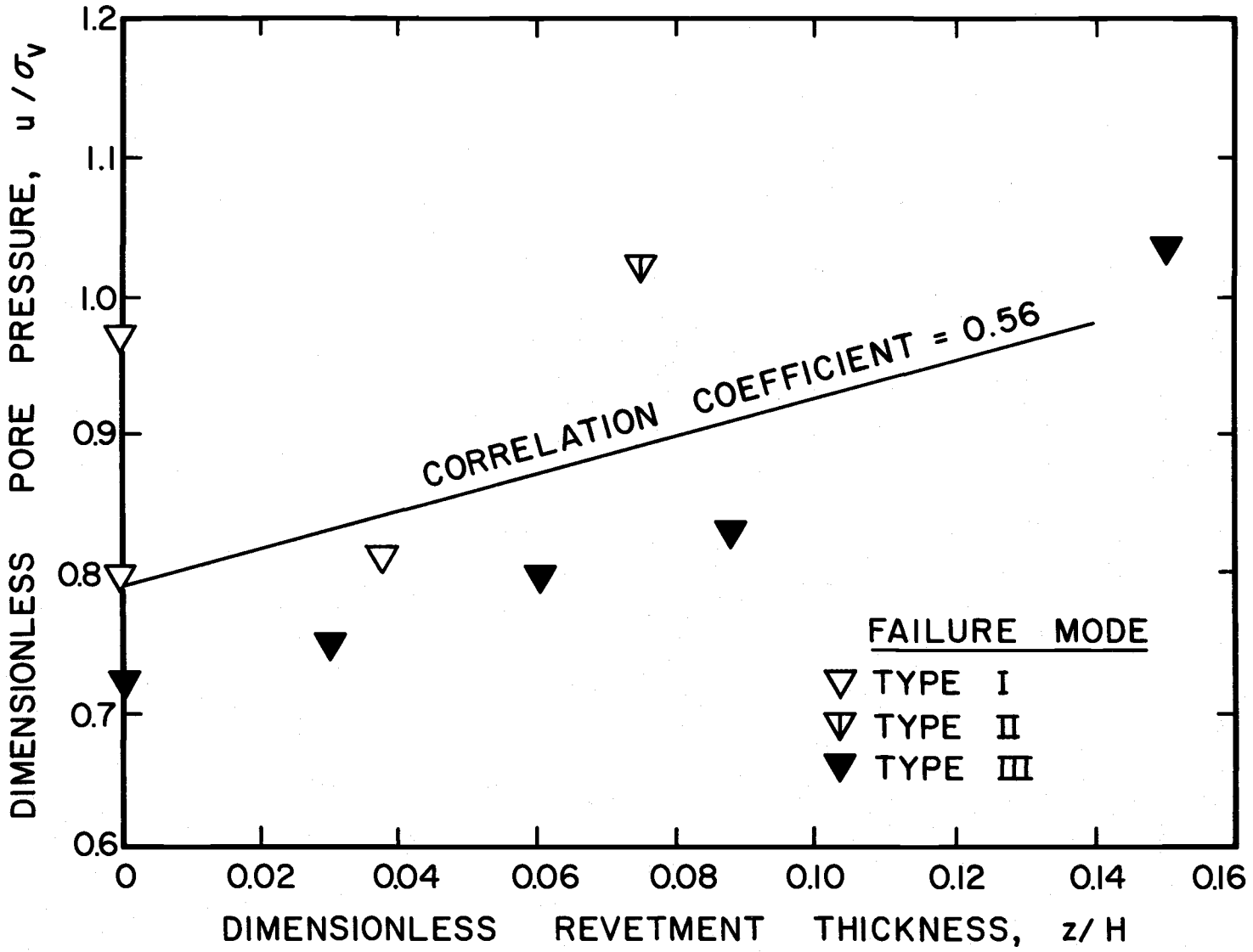

Figure 18c. Pore pressure response lower tap, B/H = 2.5.

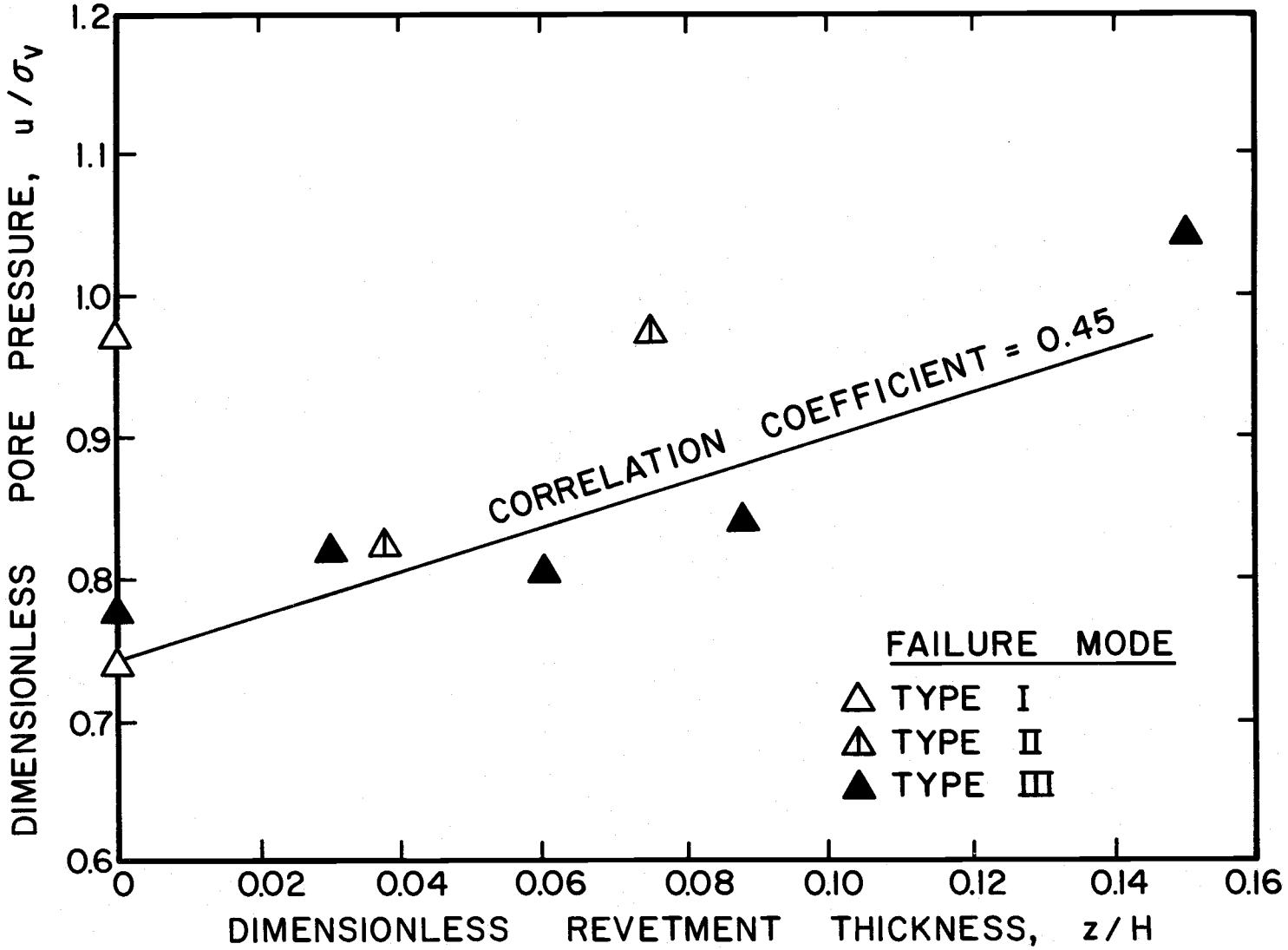

Figure 18d. Pore pressure response lower tap, B/H = 3.0.

high as 1.1 it was concluded that a gross error had been made in instrument calibration for those tests. Accordingly, all of the points for the 80 cm slopes were lowered an equal amount to make the largest values of u/σ_v equal to one. The instruments were recalibrated and the remainder of the tests showed consistent results. The plots in Figures 17 and 18 show the data after correction.

The vertical pressure σ_v was calculated from measured values of water height and soil depth at the depth of a piezometer tap. An average dry density of 92 pcf was calculated from density profiles. Even though it was impossible to quantify density in a totally accurate manner, the values of density could vary by $\pm$ 3 pcf without affecting the values of σ_v significantly.

After examining the data in Figures 17 and 18 a possible linear relationship was noted for the pore pressure stability factor plotted against z/H and B/H. In order to test this hypothesis a straight line function was fitted to these data points using least squares regression analysis. The resulting straight line functions are shown on Figures 19 and 20 for both top and bottom piezometer taps. Correlation coefficients are shown for each line and indicate the ability of the line to represent the scattered data. A coefficient of one indicates that all data points fell on the line. It can be seen that values of correlation coefficient range between 0.63 and 0.86 for the upper tap while values range between 0.43 and 0.56 for the lower tap. This

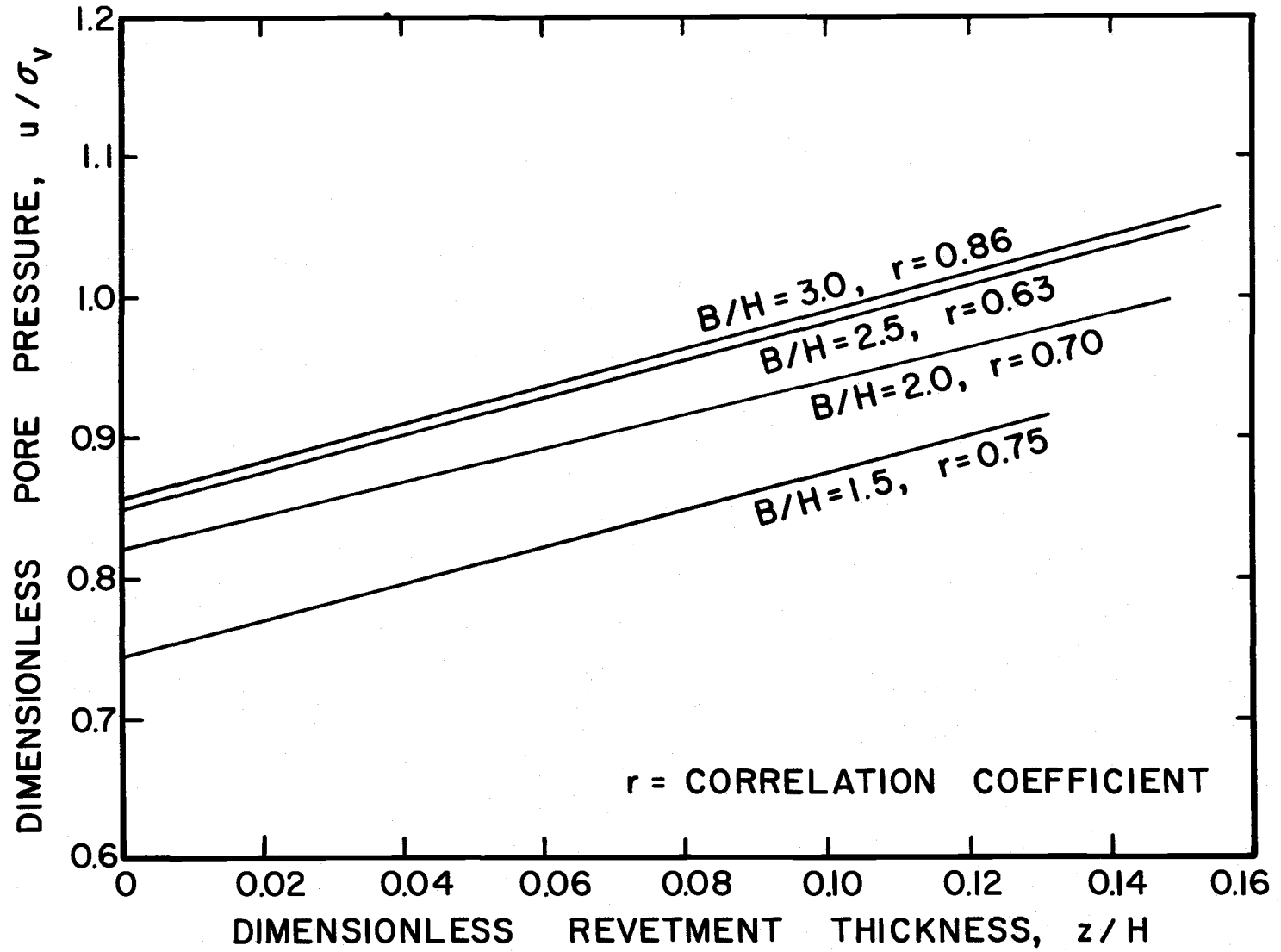

Figure 19. Least square curves for upper tap pore pressure response.

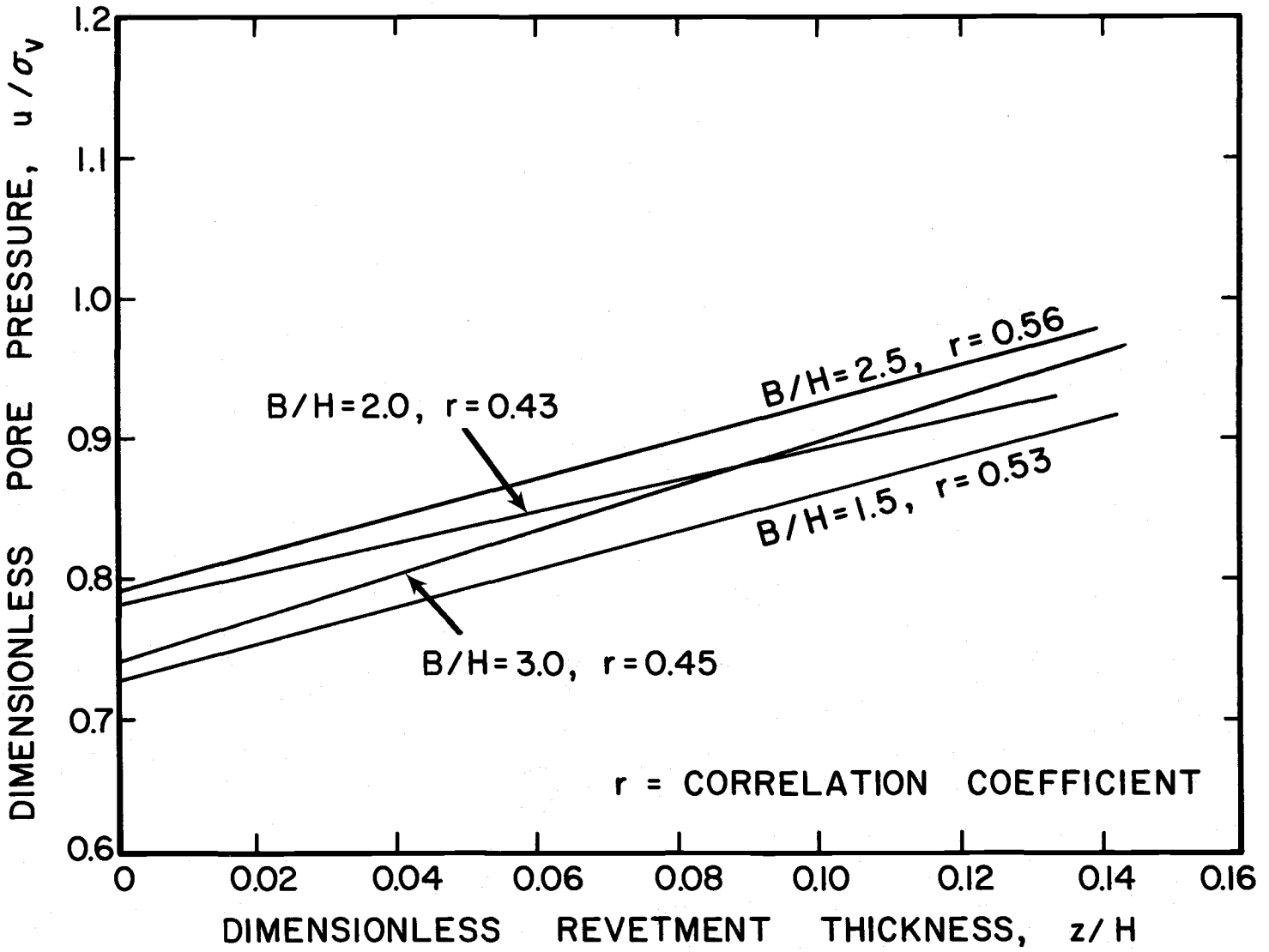

Figure 20. Least square curves for lower tap pore pressure response.

information shows that there was relatively less scatter in upper tap data and that a straight line represents a fair to good fit for this information. Apparently the lower tap data were extremely scattered and any trend that might be defined for this information should be viewed with caution.

In general, however, it is possible to define some interesting trends from the information in Figures 17 and 18, 19 and 20. It should be noted that pore pressure response showed an increase for two different conditions:

1) Pore pressure increased linearly for increasing values of revetment thickness at constant B/H.
2) Pore pressure increased for increasing values of B/H for a constant revetment thickness (upper tap only).

It is interesting to note that the response described in 1) above is opposite of the pore pressure response one would anticipate from results of repetitive load triaxial tests already described. Since increasing the value of z/H amounts to increasing the confining pressure, according to the triaxial results, the pore pressure response should have decreased with increasing revetment thickness. It is not difficult to believe that a real slope could show such opposite behavior considering that the boundary conditions are so radically different for triaxial tests. Explaining why the slope behaved as it did is another problem, however.

It seems logical that for the same B/H increasing z/H should increase the pore pressure response. With the initiation of shaking, the structure of a very loose sand is immediately broken down by the instantaneous large strains produced by the vibrating plate. The sand tries to compact but drainage has not been sufficient at this point to permit a decrease in volume of the soil structure and so the pore pressure must increase. When the sand near the top surfaces of the slope liquefied, as it always did, the weight of the surcharge had to be carried by the pore water. The value of the pore water pressure, then, not only reflected the tendency for volume change but also the magnitude of the free draining surcharge.

In a stress controlled repetitive triaxial test this same phenomenon cannot take place since the load initially imparts very small strains on the sample. Only after the soil structure has been broken down by repeated loading can the pore pressure rise to the maximum value of the external confining pressure. An increase in the confining pressure further increases the strength of the soil thus making more difficult large strains that might break down the structure of the entire soil mass. With increasing confinement the soil retains enough strength to prevent large strains from taking place at all and liquefaction can be prevented entirely.

It was probable that the magnitude of the strains induced by the plate vibrator in these models was sufficient to produce a complete

instantaneous breakdown in the loose sand structure which then permitted the buildup of larger pore pressure as the weight of larger surcharges was transferred to the pore water. However, it is also to be expected that the time rate of drainage would affect the maximum value of pore water pressure. If the drainage rate were slow, the pore pressure should have taken a longer time to build up and should have reached a larger maximum value (limited, of course, by the attainment of full liquefaction). Perhaps in this light, it is significant to note that the maximum value of pore pressure occurred within 2-3 seconds after the initiation of shaking in all tests. Within this short time span it is probable that drainge would have a minimal effect on the maximum pore pressure value even in the small model slopes.

Besides the effect of confining pressure, it was also noted that maximum values of pore pressure increased with increasing values of B/H. Although this trend could not be identified in the lower tap data due to the scatter, it could be clearly recognized in the upper tap data. This does substantiate the finding of laboratory triaxial tests in which pore pressure response increased with decreasing ratios of effective principal stress ratio, although for these model slopes the effect of slope angle was small in comparison to effect of confining pressure. It can be seen from Figure 19 that the maximum change in u/σ_v between the extremes of the smallest and largest slope angle is much smaller than the maximum change in the pore pressure response

between the extremes of revetment thickness for a single slope angle.

Further scrutiny of the pore pressure data indicates that the slopes never liquefied at a depth greater than 0.87H (which corresponds to the depth of the lower tap). The limits of the depth of liquefaction can also be defined from the upper tap pore pressure data which indicate that liquefaction reached a depth of 0.25H only for slopes with B/H values of 2.5 and 3.0 and revetment thickness of 6 cm. It is noteworthy that this maximum depth of liquefaction occurred for only Type II and III failure modes and that, therefore, limited movement of the slope and large confining pressure combined to produce the greatest extent of liquefaction.

The previous discussion of the pore pressure results has been based on the observation that least squares analysis permitted describing u/σ_v as a linear function of B/H and z/H. In order to judge the validity of describing the data in this way some accounting had to be made for the scatter in the data. When the deflection data were analyzed previously it should be recalled that an attempt was made to normalize the data by applying factors to the dimensionless parameter $\Delta H/H$ to provide similarity in the acceleration generated to fail slopes of different heights. Accordingly, an attempt was also made to normalize the pore pressure response. The normalization of the pore pressure stability factors required that u/σ_v be divided by a

constant representing the different values of acceleration and frequency measured for each of the three heights of slope. This should have reduced the scatter. When the normalization attempt was made, the data scatter increased preventing any type of curve fitting analysis. This result combined with the fact that a linear pore pressure stability function could be reasonably approximated by data, without correcting for the scale effects of acceleration, indicated that the pore pressure response was not a function of acceleration at the level of excitation used in the model tests.

To support this hypothesis it was noted that acceleration of the vibrating plate was 2, 3, and 6 times the acceleration of gravity for H = 40, 80, and 100 cm respectively. These were rather high values and the strains produced in the slopes were large enough to induce liquefaction in all of the slopes tested. It appears likely, however, that the only importance of these large strains was their ability to break down the grain to grain contacts which initiated pore pressure rise due in the slope. Since the pore pressure response did not vary radically with the large changes in acceleration for different slope heights, it must be assumed that the energy supplied by the plate beyond that needed to initiate densification did not effect the pore pressure increase measured at the taps. Apparently the energy was either absorbed by the liquefied part of the slope, effectively damping the strains that could reach the rest of the slope, or it was small in

comparison to that needed to keep the grain contacts broken and prevent compaction, after drainage became effective. In any case, the acceleration of the slopes in this study did not noticeably effect the pore pressure response. Therefore, the plots in Figures 17 and 18 were not normalized for acceleration.

Another attempt was made to reduce the scatter in the pore pressure data by accounting for variations in the density profile. The testing of several slopes which were identical except for differing density showed that values of u/σ_v could vary by as much as 10 percent. However, an attempt to quantify this change could not be accomplished because the density profile proved to be too erratic to represent. Therefore, the data were not corrected and some of the scatter was very probably due to density variations.

VI. POSSIBLE DESIGN APPLICATIONS

The knowledge that revetted model slopes behave in three very distinct ways when subject to vibration, and that it is possible to entirely prevent general flow failues using a large enough revetment invites the development of some method of slope analysis which might be used to design full scale slope revetments. This, of course, implies that full scale behavior is the same as that of model slopes and is initiated by similar response to shaking. If a theory is to be formulated, two separate cases have to be considered. It would be desirable to be able to design a revetment to completely resist lateral movement in the slope. On the other hand, it would be desirable to know the consequences of providing a revetment with a thickness smaller than that required to prevent lateral movement. The first case represents the Type III behavior observed in the model slopes. Assuming some type of failure mechanism based on the behavioral data, it should be possible to find some revetment thickness, z, required to prevent lateral slope movement, if liquefaction develops to a known depth in the slope. The approach to this problem that will be developed later is based on the simple slope stability analysis method for a sliding block failure. The second case for analysis is represented by both the Type I and Type II behavior modes observed

in the models. The Type I model is probably the more important of the two because it results in more dramatic movements.

To begin with the first case, it must be known that the revetment will be thick enough to prevent flow on the face of the slope. This assures that if failure occurs it will have to be a sliding block failure characteristic of the Type III mode. When a Type III condition is assumed initially, liquefaction begins at the top of the slope behind the crest and proceeds downward into the slope after some short period of time. As long as the slope immediately beneath the revetment does not liquefy, the revetment will act like a dam to resist the lateral force of the part of the slope that does liquefy. The liquefaction may proceed to some finite depth without producing failure in the slope unless the lateral force of the liquefied portion of the slope exceeds the shear force at the bottom of the resisting wedge provided by the revetment on non-liquified slope. As soon as the lateral driving force exceeds the resisting shear force, the wedge must slide resulting in a general flow failure. Since the shear strength at the bottom of the wedge is related to the revetment thickness, and since the driving force is related to the depth of liquefaction, it is possible to relate these two quantities at the point in time when the resisting shear force just equals the driving force.

In the analysis proposed, the following variables are defined:

h = depth of liquefaction

γ_1 = unit of weight of revetment

ϕ'_1 = effective angle of internal friction, revetment

γ_2 = unit weight of sand

ϕ'_2 = effective angle of internal friction, sand

β = angle of slope face to horizontal

z = thickness of revetment measured vertically

γ'_1, γ'_2 = buoyant unit weight of previously defined quantities

γ_w = unit weight of water

The assumptions required for this theory must now be given. Reference is made to Figure 21. First, some boundary must be chosen for the fluid - non-fluid interface. It was noted that liquefaction did not take place to the left of plane GD in Figure 21 and therefore, for convenience, that plane was chosen as the interface. The location of the interface controls the weight of the sliding wedge and the length of the sliding plane. Second, in order to calculate the effective stress along the potential failure plane along the base of the wedge some distribution of pore pressure had to be assumed. The boundary conditions dictated that the pore pressure at point D should be equal to hydrostatic pressure plus the pressure change needed to reduce the effective stress due to the buoyant weight of the sand above that point to zero. At point B the pore pressure must, of course, be hydrostatic pressure since the gravel revetment is free draining. For simplicity a linear distribution of pore pressure was assumed between these extremes.

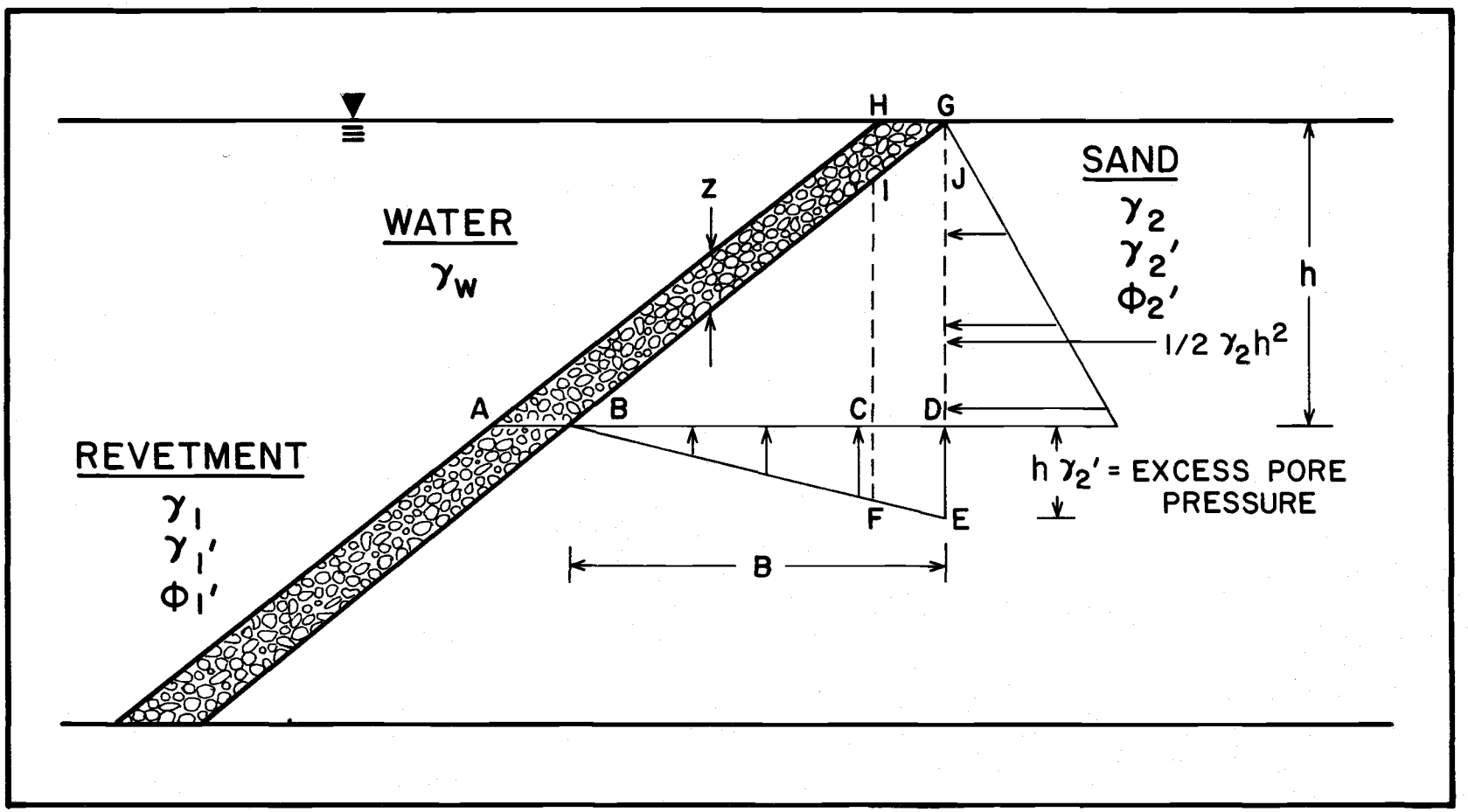

Figure 21. Sliding block analogy.

The forces on the sliding wedge AHGD are shown on Figure 21. The driving force is the lateral force produced by the liquefied sand acting on plane GD and equals $1/2\ \gamma_2 h^2$ where the unit weight of the liquefied mass is taken as the total unit weight of the saturated sand. The resisting force on plane BD was calculated in parts using the Coulomb strength equation, $s = \bar{\sigma}' \tan \phi'$, where $\bar{\sigma}'$ is the effective stress on the plane and ϕ' is the angle of internal friction of the sand or the revetment material. The effective stress on plane CD was calculated by subtracting the boundary neutral force from the weight of the soil and revetment above CD. The weight of the soil above CD equals:

$$W_{CD} = \frac{1}{\tan \beta} \left[z^2 \left(\frac{\gamma_1+\gamma_2}{2}\right) + \gamma_2 (zh-z^2) \right]$$

The boundary neutral force, U_s, on plane CD can be determined:

$$U_s = \frac{zh\gamma_w}{\tan \beta} + \frac{\gamma_2' z\, h}{\tan \beta} - \frac{\gamma_2' z^2}{2 \tan \beta}$$

Therefore the effective force on CD is

$$R_{CD} = \frac{\tan \phi'}{\tan \beta} \left[z^2 \left(\frac{\gamma_1+\gamma_2}{2}\right) + \gamma_2 (zh-z^2) \left(h\gamma_w z+\gamma_2' zh - \frac{\gamma_2' z^2}{z}\right)\right]$$

Similarly the resisting force on BC equals

$$R_{BC} = \frac{\tan \phi'}{\tan \beta} \left[\left(\frac{(h-z)^2}{2} \cdot \gamma_2 + (hz-z^2)\gamma_1 - (h\gamma_w (h-z) + \gamma_2' \frac{(h-z)^2}{2}\right)\right]$$

And the resisting force on AB equals

$$R_{AB} = \frac{z^2 \gamma_1'}{2} \frac{\tan \phi'}{\tan \beta}$$

For a factor of safety of one (critical case) the driving force equals the resisting force

$$\frac{1}{2} \gamma_2 h^2 = \frac{\tan \phi'}{\tan \beta} [z^2 \frac{(\gamma_1+\gamma_2)}{2} + \gamma_2(zh-z^2) - (h\gamma_w z+\gamma_2' zh - \frac{\gamma_z'^2}{2})]$$

$$+ \frac{\tan \phi'}{\tan \beta} [\frac{(h-z)^2}{2} \gamma_2 + (hz-z^2)\gamma_1 - (h\gamma_w(h-z)$$

$$+ \gamma_2 \frac{(h-z)^2)}{2}] + \frac{\tan \phi'}{\tan \beta} \frac{z^2 \gamma_1'}{2}$$

Collecting terms and simplifying leaves

$$\frac{\tan \beta}{\tan \phi'} \frac{1}{2} \gamma_2 h^2 = z^2 (\frac{-\gamma_w}{2}) + z\gamma h_1 - h^2 \frac{\gamma_w}{2}$$

which further reduces to the quadratic in z

$$(\frac{\gamma_w}{2}) z^2 - h \gamma_1 z + h^2 [(\frac{\gamma_2}{2} \frac{\tan \beta}{\tan \phi'} + \frac{\gamma_w}{2}] = 0 \qquad (2)$$

For known or assumed values of γ_1, γ_2, γ_w, $\tan \beta$ and $\tan \phi'$ the solution of Eq. (2) is

$$z = \text{constant } h$$

Physically, this result indicates that z must be a particular minimum thickness to prevent a sliding block failure if liquefaction develops to the maximum depth, h. Values of z can be calculated for different values of the slope angle and the angle of friction of the sand, and the

results can be plotted as shown in Figure 22. The required z as some of fraction h increases linearly with increases in the tangent of the slope angle and increases with decreasing angle of friction along the sliding plane. Using Figure 22 it is possible to design or evaluate a revetment for any assumed depth of liquefaction.

When the previously developed theory was applied to the test results, the thickness of the actual revetments which failed with Type III failures was smaller than the critical thickness indicated from the theory. The data for comparison are shown in Table 2. The information in the table indicates that, for a particular revetment thickness, the calculated depth of liquefaction needed to produce a sliding block failure was smaller than the observed depth of liquefaction. This shows that the sliding block analogy is conservative for the model slopes since the slopes liquefied to a depth greater than the critical depth without failure. It was difficult to draw these conclusions since the depth of liquefaction had to be approximated from observations and the data showing rise of the pore pressure. But it is apparent that the theory is at least conservative for the model slopes that behaved in the Type III mode. The assumptions used in deriving the theory are, of course, simplifications, but do result in a solution whith fits the results of the model tests reasonably well. The usefulness of the theory would therefore appear to depend on how well the model slope behavior is indicative of full scale slope movement.

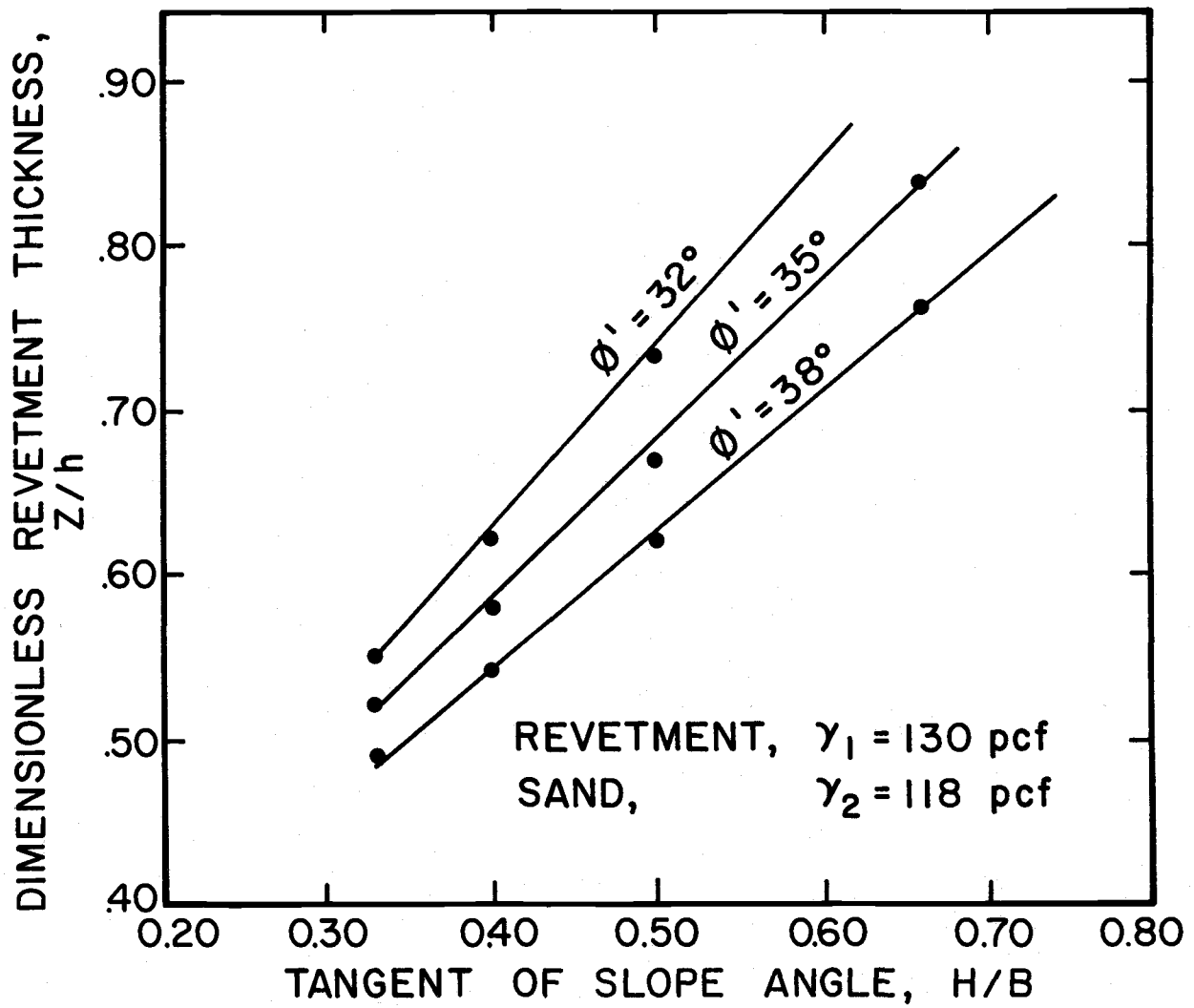

Figure 22. Solution to equation (2), required z to prevent liquefaction flow.

Table 2. Comparison of actual estimated depth of liquefaction with calculated depth of liquefaction needed to produce flow slide with given revetment thickness. Type III failures.

Slope height, h (cm)	Slope angle (B/H)	Revetment thickness, z (cm)	Estimated depth of liquefaction, h (cm)	Calculated depth of liquefaction, h (cm)
40	1.5	6	14	7.5
	2.0	6	14	9.0
	2.5	6	14	10.3
	3.0	6	14	11.6
80	2.0	6	29	9.0
	2.5	6	29	10.3
	3.0	6	29	11.6
100	1.5	6	15	7.5
	2.0	3	15	9.0
	2.0	6	15	9.0
	2.5	0	15	-
	2.5	3	15	10.3
	2.5	6	15	10.3
	3.0	0	15	-
	3.0	3	15	11.6
	3.0	6	15	11.6

The second case is the limiting condition wherein the revetment is not thick enough to prevent flow on the slope face. This case could be analyzed as a slope stability problem with a failure surface parallel to the slope face if the effective stress on the failure plane could be determined. The pore pressure has to be known to calculate the effective stress on this failure plane and it was not measured in the tests described earlier. All that is known is that the Type I failure mechanism, observed and previously described, does occur.

It was noted, however, that in all cases where a Type I failure occurred, it could be verified as shown on Table 3, that the depth of liquefaction exceeded h, the depth of liquefaction needed to produce a sliding block failure with a particular thickness of revetment z. The problem thus presented is to use this observation to recommend a procedure for choosing a minimum thickness, z, to effect a satisfactory design. Lacking a more rational approach, the judgment may be made that since the slope face flow only occurs when initiated by a sliding block failure, it is logical to design to prevent the sliding block failure and thereby preclude the face flow.

The simplifying assumptions notwithstanding, the sliding block analysis provides a useful means of linking observed failure modes derived from the model tests with a practical way of designing full size slopes. Assuming that the model test failure modes are representative of what will happen in a similar full scale slope and assuming

Table 3. Comparison of actual estimated depth of liquefaction with calculated depth of liquefaction needed to produce flow slide with given revetment thickness. Type I failures.

Slope height, h (cm)	Slope angle (B/H)	Revetment thickness, z (cm)	Estimated depth of liquefaction, h (cm)	Calculated depth of liquefaction, h (cm)
40	1.5	0	7	-
	1.5	3	8	3.6
	2.0	0	7	-
	2.0	3	5	4.5
	2.5	0	6	-
	3.0	0	5	-
80	1.5	0	15	-
	1.5	3	15	3.6
	2.0	0	9	-
	2.0	3	6	4.5
	2.5	0	7	-
	2.5	3	6	5.2
	3.0	0	5	-
100	1.5	0	5	-
	1.5	3	10	3.6
	2.0	0	5	-

that a revetment is thick enough to prevent the gravity flow of material down the face of the slope, the curves in Figure 22 show that z for the revetment would have to be at least .80 of the possible depth of liquefaction to prevent horizontal slope movement. This means that if the slope liquefied to its full depth, the revetment would have a z equal to .80 of the height of the slope. In a large slope with a correspondingly large revetment, liquefaction potential within the proximity of the revetment would be reduced by the presence of the free draining surcharge or confining stress in the underlying layers of sand. If the in situ strength of the sand deposit was much higher than the worst case assumed and the slope angle was decreased, the required z could be as small as .50 of the slope height for full depth of liquefaction. In light of the empirical nature of these results the designer would best be conservative and, when designing for the possibility of liquefaction in a moderately high slope, should assume that the slope liquefies to full depth. Revetments designed in this way would probably be conservative. Since the sliding block analysis was conservative for model slopes, some extra strength was being utilized which could not be accounted for in the analysis. This strength could have been the result of drainage, dilatancy or the effect of surcharge on liquefaction potential. Whatever the cause, it is not unreasonable to assume that the same effects might be seen in real slopes.

The previous discussion has centered on a conservative design based on the worst possibility, i.e., full depth liquefaction. A designer may not wish to use this degree of conservation in an area where some risk of damage can be tolerated or where human life will not be in danger. In this case a less conservative design would result from designing the revetment for something less than a depth of liquefaction equal to the slope height. Florin and Ivanov (6) have suggested that it would be unusual for liquefaction to occur in level sand deposits at a depth greater than about 45 feet. This information could be used as a guide for slopes with heights greater than 45 feet. A more rational way in which to determine the depth of liquefaction would be to use the procedure for evaluating liquefaction potential developed by Seed and Idriss, which compares response to cyclic stress determined in the laboratory with calculated earthquake stresses (8). Using their procedure a zone of liquefaction could be defined and used to predict the maximum depth of liquefaction in the sand material behind the slope crest. Once the depth of liquefaction has been determined, it only remains to determine the thickness of revetment needed for specific soil properties using Eq. (2).

VII. CONCLUSIONS

On the basis of model tests it has been shown that pore pressure response of model slopes can be scaled. This does not, however, lead to the conclusion that these relationships will be valid for slopes much greater in size than the largest models. In addition, in revetted model slopes, the pore pressure response to vibration has been shown to increase with increasing revetment thickness or confining pressure. This observation is in direct contrast to the judgments one would make from the results of repetitive load triaxial tests. Pore pressure response in the model slopes does verify laboratory triaxial test results in that pore pressure increased with decreasing slope angles or decreasing ratios of major to minor principal stress.

In modeling the pore pressure response, the scale effects of acceleration did not effect the linear relationship between the dimensionless revetment thickness and the dimensionless pore pressure.

In general the results of the model studies of the slopes have suggested that previous laboratory testing studies on small samples may not properly be representative of actual conditions in slopes. However, beyond defining the general trends, the pore pressure data obtained in the models cannot be used numerically until further studies can verify the relationship for large slopes.

The model studies have shown that distinct failure mechanisms do exist when a slope is subject to vibration, and that the sliding block type of analysis has been shown to fit the observed failure condition in models. Although the sliding block does not exactly represent the actual failure mode, observation of the maximum depth of liquefaction has shown that this method is conservative for model slopes. The natural extension of this theory can be used to design full size slopes. However, this kind of extrapolation should definitely be used with caution since the theory upon which it is based presumes a slope behavior mode which should be verified in observations at full scale.

It appears that the most useful part of these model studies has been the discovery of failure mechanisms. A very productive plan of future study would certainly include some refinement in the equipment to enable the development of a complete pore pressure distribution throughout the slope. With a grid of pore pressure measuring devices it would be easier to define the extent of liquefaction and at the same time allow a more complete evaluation of the effective stress anywhere within the slope. Using this information it would then be possible to better define the strength of the sand along a particular failure surface and further refine the sliding block slope stability analysis. Of course, it would be desirable to know if full scale saturated sand slopes will fail in the same failure modes

exhibited by the model slopes. In any case, future studies with refined equipment and procedures could prove useful in further defining failure mechanisms, thus allowing the development of more accurate design procedures.

BIBLIOGRAPHY

1. Finn, W.D. Liam, Pickering, D.J. and Bransby, P.L., "Sand Liquefaction in Triaxial and Simple Shear Tests," Journal of the Soil Mechanics and Foundation Division, ASCE, Vol. 95, No. SM4, Apr., 1971, pp. 639-660.

2. Florin, V.A. and Ivanov, P.L., "Liquefaction of Saturated Sandy Soils," Proceedings, Fifth International Conference on Soil Mechanics and Foundation Engineering, Vol. 1, 1961, pp. 107-111.

3. Lee, Kenneth L. and Seed, H. Bolton, "Cyclic Stress Conditions Causing Liquefaction of Sand," Journal of the Soil Mechanics and Foundation Division, ASCE, Vol. 93, No. SM1, Jan., 1967, pp. 47-70.

4. Lee, Kenneth L. and Seed, H. Bolton, "Dynamic Strength of Anisotropically Consolidated Sand," Journal of the Soil Mechanics and Foundation Division, ASCE, Vol. 93, No. SM5, Sept., 1967, pp. 169-190.

5. Peacock, William H. and Seed, H. Bolton, "Sand Liquefaction Under Cyclic Loading Simple Shear Conditions," Journal of the Soil Mechanics and Foundation Division, ASCE, Vol. 94, No. SM3, May, 1968, pp. 689-708.

6. Schroeder, W.L. and Schuster, R.L., "Liquefaction Phenomena in Saturated Sands," Proceedings, Sixth Annual Symposium on Engineering Geology and Soils Engineering, Boise, Idaho, 1968, pp. 1-22.

7. Seed, H. Bolton, "Landslides during Earthquakes Due to Liquefaction," Journal of the Soil Mechanics and Foundation Division, ASCE, Vol. 94, No. SM5, Sept., 1968, pp. 1055-1122.

8. Seed, H. Bolton and Idriss, Izzat M., "Simplified Procedure for Evaluating Soil Liquefaction Potential," Journal of the Soil Mechanics and Foundation Division, ASCE, Vol. 97, No. SM9, Sept., 1971, pp. 1249-1273.

9. Seed, H. Bolton and Peacock, W.H., "Test Procedures for Measuring Soil Liquefaction Characteristics," Journal of the Soil Mechanics and Foundation Division, ASCE, Vol. 97, No. SM8, Aug., 1971, pp.

10. Seed, H. Bolton, "Use of Simulated Earthquake Loading Conditions in Research Relating to the Seismic Behavior of Soils and Soils Structures," Earthquake Environment Simulation, National Academy of Engineering, Sept. 7-9, 1973, pp. 138-141.

11. Wen-Xi, H., "Investigations of Stability of Saturated Sand Foundations and Slopes against Liquefaction," Proceedings, Fifth International Conference on Soil Mechanics and Foundation Engineering, Paris, Vol. 2, 1961, pp. 629-631.

APPENDIX

NOTATION

A = Amplitude of particle displacement

B = Horizontal distance between slope crest and toe

g = Acceleration due to gravity

H = Height of slope

k = Permeability

r = Correlation coefficient

t = Time

u = Pore water pressure

z = Thickness of revetment

γ = Unit weight of sand

γ' = Buoyant unit weight of sand

ϕ' = Angle of internal friction of sand

γ_w = Unit weight of water

η = Frequency

λ = Scale factor

h = Depth of liquefaction

$\overline{\sigma}'$ = Effective stress

$\tan\beta$ = H/B or tangent of the slope angle

Data Summary

Figure 23 shows a typical oscillograph record for one slope failure. The two upper line traces on the top of the record indicate increased pore pressure with time. The maximum value of the pore pressure was used to determine the dimensionless pore pressure stability factor as indicated from Figure 23. It should be noted that the trace only indicates changes in pore pressure and therefore the values taken from Figure 23 represent the maximum change in pore pressure. To calculate the total pore pressure it was necessary to measure the static head and add it to the values taken from the print-out.

The bottom trace which appears sinusoidal is the record of the acceleration of the top of the vibrating plate. The acceleration was measured from the zero axis as shown in Figure 23.

Table 4 is a summary of data for all of the slope tested.

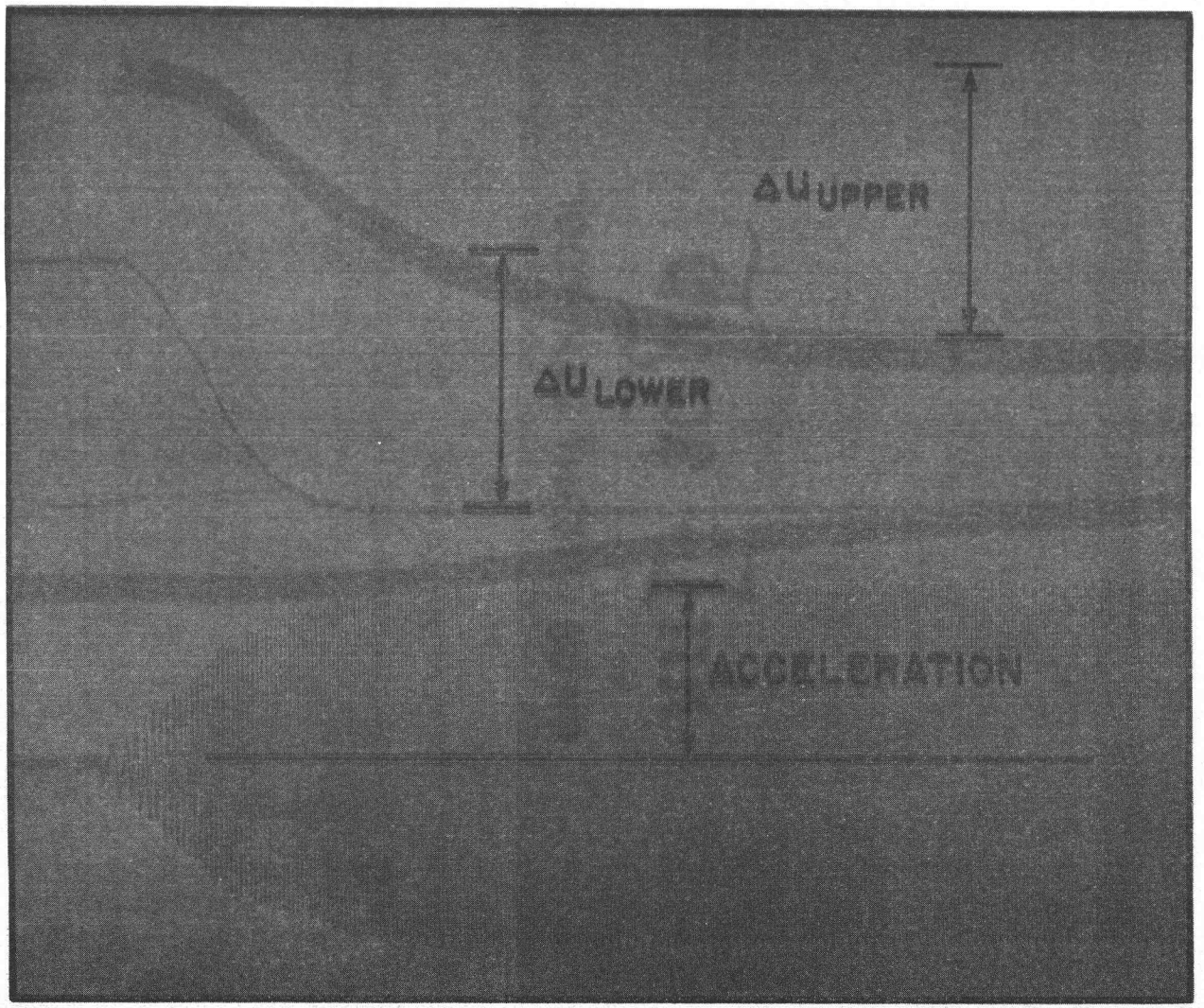

Figure 23. Oscillograph printout showing maximum pore pressure change and acceleration.

Table 4. Summary of test data.

H (cm)	B/H	z	z/H	η (Hz)	A/g	ΔH (cm)	ΔH/H	Upper tap $(\frac{u_{max}}{\sigma_v})$	Lower tap $(\frac{u_{max}}{\sigma_v})$
40	1.5	0	0	29.0	2.03	6.7	0.168	0.82	0.93
		3	0.075	28.5	1.97	6.0	0.150	0.84	0.96
		6	0.150	29.0	2.03	5.0	0.125	0.96	0.96
	2.0	0	0	27.5	2.03	8.4	0.210	0.90	1.00
		3	0.075	28.5	1.97	5.0	0.125	0.92	0.99
		6	0.150	28.0	1.89	4.8	0.120	1.03	1.02
	2.5	0	0	28.5	1.89	5.6	0.140	0.91	0.97
		3	0.075	28.0	1.89	3.2	0.080	0.99	1.02
		6	0.150	28.0	2.02	3.0	0.075	1.03	1.03
	3.0	0	0	28.0	1.89	5.5	0.138	0.89	0.97
		3	0.075	28.0	1.89	3.7	0.093	0.98	0.97
		6	0.15	28.0	2.02	3.0	0.075	1.04	1.04
80	1.5	0	0	33.3	3.07	12.5	0.156	0.752	0.675
		0	0	33.3	2.89	14.0	0.175	0.765	0.694
		3	0.0375	30.5	3.27	15.0	0.188	0.769	0.700
		3	0.0375	32.0	2.99	15.5	0.193	0.870	0.809
		7.5	0.0938	32.3	2.97	9.8	0.122	0.892	0.786
	2.0	0	0	32.0	2.70	10.0	0.125	0.870	0.771
		3	0.0375	30.5	2.70	6.5	0.081	0.910	0.793
		7	0.0875	30.0	2.70	3.5	0.044	0.940	0.778
	2.5	0	0	30.0	2.78	6.0	0.075	0.880	0.794
		3	0.0375	31.5	2.75	5.5	0.069	0.930	0.805
		7	0.0875	32.0	2.70	4.0	0.050	0.960	0.825

(Continued on next page)

Table 4. (Continued)

H (cm)	B/H	z	z/H	η (Hz)	A/g	ΔH (cm)	ΔH/H	Upper tap $(\frac{u_{max}}{\sigma_v})$	Lower tap $(\frac{u_{max}}{\sigma_v})$
80	3.0	0	0	30.0	2.86	5.0	0.0625	0.890	0.772
		3	0.0375	32.0	2.72	5.0	0.0625	0.970	0.825
		7	0.0875	31.5	2.72	3.0	0.0375	1.000	0.840
100	1.5	0	0	42.5	6.48	8.5	0.085	0.690	0.650
		3	0.03	42.5	6.48	12.0	0.120	0.730	0.790
		6	0.06	43.5	6.48	3.0	0.030	0.720	0.670
	2.0	0	0	41.5	6.48	7.0	0.070	0.750	0.720
		3	0.03	42.0	6.48	3.5	0.035	0.790	0.746
		6	0.06	42.0	6.48	2.8	0.028	0.780	0.705
	2.5	0	0	42.0	6.30	3.0	0.030	0.770	0.720
		3	0.03	42.0	6.30	2.0	0.020	0.820	0.740
		6	0.06	42.0	5.94	3.0	0.030	0.890	0.796
	3.0	0	0	40.5	5.94	3.6	0.036	0.770	0.741
		3	0.03	40.5	5.94	2.5	0.025	0.880	0.813
		6	0.06	37.5	5.40	4.0	0.040	0.925	0.807